M., Natsugari, H., Kan, T., Fukuyama, T., Tomita, T., and Iwatsubo, T. (2007) *ACS Chem. Biol.* **2,** 408–418
23. Isoo, N., Sato, C., Miyashita, H., Shinohara, M., Takasugi, N., Morohashi, Y., Tsuji, S., Tomita, T., and Iwatsubo, T. (2007) *J. Biol. Chem.* **282,** 12388–12396
24. Bergman, A., Laudon, H., Winblad, B., Lundkvist, J., and Näslund, J. (2004) *J. Biol. Chem.* **279,** 45564–45572
25. Laudon, H., Mathews, P. M., Karlström, H., Bergman, A., Farmery, M. R., Nixon, R. A., Winblad, B., Gandy, S. E., Lendahl, U., Lundkvist, J., and Näslund, J. (2004) *J. Neurochem.* **89,** 44–53
26. Zhao, B., Yu, M., Neitzel, M., Marugg, J., Jagodzinski, J., Lee, M., Hu, K., Schenk, D., Yednock, T., and Basi, G. (2008) *J. Biol. Chem.* **283,** 2927–2938
27. Shirotani, K., Edbauer, D., Capell, A., Schmitz, J., Steiner, H., and Haass, C. (2003) *J. Biol. Chem.* **278,** 16474–16477
28. Leem, J. Y., Vijayan, S., Han, P., Cai, D., Machura, M., Lopes, K. O., Veselits, M. L., Xu, H., and Thinakaran, G. (2002) *J. Biol. Chem.* **277,** 19236–19240
29. Kaether, C., Lammich, S., Edbauer, D., Ertl, M., Rietdorf, J., Capell, A., Steiner, H., and Haass, C. (2002) *J. Cell Biol.* **158,** 551–561
30. Herreman, A., Van Gassen, G., Bentahir, M., Nyabi, O., Craessaerts, K., Mueller, U., Annaert, W., and De Strooper, B. (2003) *J. Cell Sci.* **116,** 1127–1136
31. Hayashi, I., Takatori, S., Urano, Y., Iwanari, H., Isoo, N., Osawa, S., Fukuda, M. A., Kodama, T., Hamakubo, T., Li, T., Wong, P. C., Tomita, T., and Iwatsubo, T. (2009) *J. Biol. Chem.* **284,** 27838–27847
32. Saura, C. A., Tomita, T., Davenport, F., Harris, C. L., Iwatsubo, T., and Thinakaran, G. (1999) *J. Biol. Chem.* **274,** 13818–13823
33. Kim, S. H., and Sisodia, S. S. (2005) *J. Biol. Chem.* **280,** 41953–41966
34. Ratovitski, T., Slunt, H. H., Thinakaran, G., Price, D. L., Sisodia, S. S., and Borchelt, D. R. (1997) *J. Biol. Chem.* **272,** 24536–24541
35. Tomita, T., Watabiki, T., Takikawa, R., Morohashi, Y., Takasugi, N., Kopan, R., De Strooper, B., and Iwatsubo, T. (2001) *J. Biol. Chem.* **276,** 33273–33281
36. Brunkan, A. L., Martinez, M., Wang, J., Walker, E. S., Beher, D., Shearman, M. S., and Goate, A. M. (2005) *J. Neurochem.* **94,** 1315–1328
37. Erez, E., Fass, D., and Bibi, E. (2009) *Nature* **459,** 371–378
38. Annaert, W. G., Esselens, C., Baert, V., Boeve, C., Snellings, G., Cupers, P., Craessaerts, K., and De Strooper, B. (2001) *Neuron* **32,** 579–589
39. Baker, R. P., Young, K., Feng, L., Shi, Y., and Urban, S. (2007) *Proc. Natl. Acad. Sci. U.S.A.* **104,** 8257–8262

Journal of Neuroscience Research

Journal of Neuroscience Research 88:3547–3554 (2010)

Amyloid β Accelerates Phosphorylation of Tau and Neurofibrillary Tangle Formation in an Amyloid Precursor Protein and Tau Double-Transgenic Mouse Model

Yusuke Seino,[1] Takeshi Kawarabayashi,[2]* Yasuhito Wakasaya,[2] Mitsunori Watanabe,[2] Ayumi Takamura,[2] Yukiko Yamamoto-Watanabe,[2] Tomoko Kurata,[3] Koji Abe,[3] Masaki Ikeda,[4] David Westaway,[5] Tetsuro Murakami,[6] Peter St. George Hyslop,[6] Etsuro Matsubara,[2] and Mikio Shoji[2]

[1]Department of General Medicine, Mutsu General Hospital, Mutsu, Japan
[2]Department of Neurology, Hirosaki University Graduate School of Medicine, Hirosaki, Japan
[3]Department of Neurology, Okayama University Graduate School of Medicine and Dentistry, Okayama, Japan
[4]Department of Neurology, Gunma University Graduate School of Medicine, Maebashi, Japan
[5]Centre for Prions and Protein Folding Diseases, University of Alberta, Edmonton, Alberta, Canada
[6]Canada Centre for Research in Neurodegenerative Diseases, University of Toronto, Toronto, Ontario, Canada

In Alzheimer's disease, Aβ deposits are considered the initial cardinal events that induce tauopathy secondarily. However, the relationship between Aβ amyloidosis and tauopathy has not been determined in detail. We produced double transgenic mice, 2×TgTau$^{+/-}$APP$^{+/-}$, by mating Tg2576 mice that exhibit Aβ amyloidosis and TgTauP301L mice that show tauopathy, and statistically analyzed the effect of Aβ accumulation on tauopathy. There was no significant difference in the progression of Aβ accumulation among 2×TgTau$^{+/-}$APP$^{+/-}$ and 1×TgTau$^{-/-}$APP$^{+/-}$, and tau accumulation among 2×TgTau$^{+/-}$APP$^{+/-}$ and 1×TgTau$^{+/-}$APP$^{-/-}$. The appearance rates of phosphorylated tau developing in neurons and processes were significantly accelerated in 2×TgTau$^{+/-}$APP$^{+/-}$ mice compared with those in 1×TgTau$^{+/-}$APP$^{-/-}$ mice at 23 months of age. Accumulation of phosphorylated and confomationally altered tau and GSK3β in neuronal processes was accelerated in the white matter in 2×TgTau$^{+/-}$APP$^{+/-}$. The level of phosphorylated tau in the sarkosyl-insoluble fraction was increased in 2×TgTau$^{+/-}$APP$^{+/-}$ brains compared with that in 1×TgTau$^{+/-}$APP$^{-/-}$ brains. Thus, Aβ amyloid partially enhances tauopathy through accumulation of insoluble, phosphorylated, and conformationally changed tau in neuronal cytoplasm and processes in the late stage. © 2010 Wiley-Liss, Inc.

Key words: Alzheimer's disease; double transgenic mouse; neurofibrillary tangles

Alzheimer's disease (AD) brains are invariably characterized by two pathological features, initial Aβ amyloidosis by extracellular deposition of Aβ and subsequent intracellular accumulation of neurofibrillary tangles (NFTs) comprising abnormal aggregates of phosphorylated tau. Aβ cascade from Aβ deposits to the final appearance of tauopathy and neuronal cell losses is the major hypothesis that explains all steps in the pathogenesis of AD. Soluble Aβ oligomers are considered the cardinal molecules that adversely affect synaptic structures and plasticity (Hardy, 2009). Tauopathy is present in sporadic frontotemporal dementia such as progressive supranuclear palsy and corticobasal degeneration and caused by MAPT gene mutation itself in FTDP-17 (Hutton et al., 1998). Other types of diseases such as brain amyloids of familial British dementia (Ghiso et al., 2001) and lysosomal disorders of Niemann-Pick disease type C also induce numerous NFTs (Love et al., 1995). Because JNPL3 mice expressing double APP and tau mutations exhibited substantial enhanced NFT pathology in the limbic system and

Contract grant sponsor: Ministry of Health, Labor and Welfare of Japan; Contract grant number: 19390233 (to M.S.); Contract grant number: 19590976 (to T.Ka.); Contract grant number: 18590968 (to E.M.); Contract grant sponsor: Ministry of Education, Culture, Sports, Science and Technology, Japan (to M.S.); Contract grant sponsor: The Mochida Memorial Foundation for Medical and Pharmaceutical Research (to M.W.); Contract grant sponsor: Hirosaki University Institutional Research (to M.S.).

*Correspondence to: Takeshi Kawarabayashi, Department of Neurology, Institute of Brain Science, Hirosaki University Graduate School of Medicine 5 Zaifucho, Hirosaki 036-8562, Japan.
E-mail: tkawara@cc.hirosaki-u.ac.jp

Received 12 May 2010; Revised 5 August 2010; Accepted 17 August 2010

Published online 8 October 2010 in Wiley Online Library (wileyonlinelibrary.com). DOI: 10.1002/jnr.22516

olfactory cortex (Lewis et al., 2001), investigations into mechanisms underlying Aβ induced tauopathy have been facilitated. Accumulation of phosphorylated tau was enhanced around senile plaque cores (Tomidokoro et al., 2001). Injection of Aβ42 fibrils or brain Aβ extracts into the brains of the tau transgenic mice models caused increases in the number of NFTs (Götz et al., 2001). Administration of Aβ antibodies cleared Aβ deposits and delayed subsequent tauopathy in a 3×Tg-AD mouse model (Oddo et al., 2004). Blocking Aβ42 or Aβ oligomer accumulation delayed the onset and progression of tau pathology (Oddo et al., 2008). Reduction of both soluble Aβ and tau levels have been suggested as necessary to rescue cognitive impairment in 3×Tg-AD model mice (Oddo et al., 2006a). In contrast, augmenting tau levels did not modulate the onset or progression of Aβ pathology (Oddo et al., 2007). Thus, a unidirectional mechanism from Aβ amyloids to tauopathy is suggested in transgenic mouse models. However, follow-up of a phase I trial of immunization with Aβ42 did not prevent clinical progression of dementia, tauopathy, or neuronal cell loss, even though it resulted in the clearance of amyloid plaques (Holmes et al., 2008). These findings have facilitated further clarification of the precise mechanisms underlying induction of tauopathy by Aβ amyloidosis.

We have established a tauopathy model mouse expressing 2N4R human tauP301L (TgTauP301L), which develops a florid pathology that includes numerous pretangles, NFTs, and glial fibrillary tangles (GFTs) in the frontotemporal areas of the cerebrum, accompanied by gliosis, neuronal loss, and cerebral atrophy. Accumulated tau was hyperphosphorylated, conformationally changed, ubiquitinated, and sarkosyl insoluble. These mice exhibited impairment in hippocampus-dependent and -independent behavioral paradigms and showed substantial phenotypic variation and a spectrum of pathologies similar to that observed in FTDP-17 patients (Murakami et al., 2006). Here, we generated double transgenic mice, $2\times TgTau^{+/-}APP^{+/-}$, by mating Tg2576 mice that exhibit marked Aβ deposits (Kawarabayashi et al., 2004) with TgTauP301L mice in order to analyze how Aβ amyloids induces tauopathy. Progression of deposits of Aβ, phosphorylated and conformatinally changed tau, NFTs, GFT, and phenotypic variation were compared among $2\times TgTau^{+/-}APP^{+/-}$, $1\times Tau^{+/-}APP^{-/-}$, $1\times TgTau^{-/-}APP^{+/-}$, and $0\times TgTau^{-/-}APP^{-/-}$ mice. Although there were no significant changes in the progression of Aβ and tau deposits from 8 to 16 months of age, the presence of phosphorylated and conformationally changed tau in dystrophic neurites around senile plaques and neuropil threads and the appearance of pretangles and NFTs were significantly enhanced in $2\times TgTau^{+/-}APP^{+/-}$ at 23 months of age. Based on these findings, the acceleration of tauopathy by Aβ amyloidosis was considered slow and not very strong, requiring a long incubation period during which phosphorylation, conformational change, and insolubilization of tau occurred.

MATERIALS AND METHODS

Transgenic Mouse Models

To generate double transgenic mice expressing tauP301L and βAPP KM670/671NL, TgTauP301L maintained in the FVB/N strain were mated with Tg2576 mice maintained in the B6/SJL strain and defined as $2\times TgAPP^{+/-}Tau^{+/-}$. Heterozygote F1 littermates of TgTauP301 and Tg2576 were used for all experiments to analyze uniform genetic background mice as FVB/B6/SJL. Each genotypic strain was $2\times TgTau^{+/-}APP^{+/-}$ expressing human 2N4R tauP301L and βAPP KM670/671NL, $1\times TgTau^{+/-}APP^{-/-}$, $1\times TgTau^{-/-}APP^{+/-}$, and $0\times TgTau^{-/-}APP^{-/-}$, which was the wild FVB/B6/SJL mouse expressing only endogenous mouse APP and tau. In total 124 mice were examined. Twenty-three $2\times TgTau^{+/-}APP^{+/-}$ (3 mice at 8 months of age, 4 mice at 12 months, 6 mice at 16 months, and 8 mice at 23 months), 62 $1\times TgTau^{+/-}APP^{-/-}$ (7 mice at 8 months, 15 mice at 12 months, 27 mice at 16 months, and 13 mice at 23months), 16 $1\times TgTau^{-/-}APP^{+/-}$ (1 mouse at 8 months, 1 mouse at 12 months, 5 mice at 16 months, and 9 mice at 23 months), and 23 $0\times TgTau^{-/-}APP^{-/-}$ (16 mice at 8 months, 1 mouse at 12 months, 19 mice at 16 months, and 4 mice at 23 months) were analyzed. All animal experiments were performed according to guidelines established in the Guide for the care and use of laboratory animals and the ethical committee of Hirosaki University.

Immunostaining

After mice were sacrificed under ether anesthesia, brains were removed and cut sagitally along the midline. One hemisphere was fixed in 4% paraformaldehyde with 0.1 M phosphate buffer (pH 7.6) for 8 hr and embedded in paraffin. Five-micrometer-thick sections were prepared for immunostaining and Gallyas-Braak silver stain. Sections were immersed in 0.5% periodic acid to block intrinsic peroxidase and treated with 99% formic acid for 3 min. Microwave pretreatment was used for AT8 staining. After blocking with 5% normal goat or horse serum in 50 mM phosphate-buffered saline (pH 7.4) containing 0.05% Tween 20 and 4% Block Ace (Snow Brand, Sapporo, Japan), sections were incubated overnight with primary antibodies. Specific labeling was visualized by Vectastain Elite ABC kit (Vector, Burlingame, CA). Tissue sections were counterstained with hematoxylin. The following antibodies were used in this study: tau-154, against amino acids 154–168 of human tau441 that specifically detect human tau (1:200); HT7. against amino acids 159–163 of human tau441 that specifically detect human tau (1:500; Innogenetics, Gent, Belgium); CP27, against all forms of human tau (1:500); TAU-5, against amino acids of human tau441 that detects both human and mouse tau (1:1,000; Abcam, Cambridge, MA); MC1, against early epitope of confomationally changed tau (1:400); PS199, against phosphorylated tau at serine199 (1:500); CP13, against phosphorylated tau at serine202 (1:400); AT8, against phosphorylated tau at serine202/threonine205 (1:400; Innogenetics); anti-PT231/PS235, against phosphorylated tau at threonine231/serine235 (1:500); PHF-1, against phosphorylated tau at serine396/serine404 (1:400); anti-PS413, against phosphorylated tau at serine413 (1:100);

Ab9204, against N-terminal aspartate of Aβ (0.1 μg/ml); and anti-GSK3β antibody (1:100) were used (Tomidokoro et al., 2001).

Western Blot

The other half of the mouse brain was weighed and homogenized using a motor-driven Teflon glass homogenizer for 20 strokes in 9 volumes of Tris-saline buffer (TS) with protease inhibitors (TS inhibitors 50 mM Tris-HCl and 150 mM NaCl, pH 7.6, with protease inhibitor cocktail; Complete; Roche Diagnostics, Indianapolis, IN). The homogenate was centrifuged at 55,000 rpm for 60 min at 4°C, and the supernatant was analyzed as the TS-soluble fraction. After washing with 10 volumes of TS with protease inhibitors, the pellet was homogenized again in 4 volumes of 1% sarkosyl in TS inhibitors, incubated on ice for 30 min, and centrifuged at 55,000 rpm for 60 min at 4°C. The supernatant was analyzed as the sarkosyl-soluble fraction. The pellet was washed twice with 10 volumes of 1% sarkosyl in TS inhibitors, and the remaining pellet was analyzed as the sarkosyl-insoluble fraction. Each sample was boiled at 70°C in SDS sample buffer, separated on 4–12% NuPAGE Bis-Tris Gel (Invitrogen, Carlsbad, CA), and electrotransferred to Immobilon P (Millipore, Bedford, MA) at 100 V for 1.5 hr. The blots were labeled by HT-7, Tau5, PHF-1, AT8, and CP13. The signal intensity of labeled protein using Supersignal (Pierce, Rockford, IL) was quantified by the luminoimage analyzer (LAS 1000-Mini; Fuji Film, Tokyo, Japan).

RESULTS

Appearance of expressed human tauP301L began at 3 months of age in both $2\times TgTau^{+/-}APP^{+/-}$ and $1\times TgTau^{+/-}APP^{-/-}$. With aging, the human tauP301L accumulated progressively and distributed widely from the hippocampus to the cerebral cortices, thalamus, amygdale, striatum, and brainstem. There were no significant differences observed in initiation, distribution, and progression of human tauP301L accumulation between $2\times TgTau^{+/-}APP^{+/-}$ (Fig. 1a–d) and $1\times TgTau^{+/-}APP^{-/-}$ (Fig. 1e–h). Neither brain atrophy nor hydrocephalus was observed in either group. Progressive accumulation of endogenous mouse tau was also detected by TAU-5 immunostaining in relation to the expressed human tauP301L accumulation. There were no significant differences in brain gliosis, neuronal cell loss, behavioral disturbance, or survival between $2\times TgTau^{+/-}APP^{+/-}$ and $1\times TgTau^{+/-}APP^{-/-}$ However, marked accumulation of phosphorylated tau was detected by AT8 immunostaining in the hippocampus and the cerebral cortices in $2\times TgTau^{+/-}APP^{+/-}$ mice compared with $1\times TgTau^{+/-}APP^{-/-}$ mice at 23 months age (Fig. 1l). This accumulated tau was partially labeled by Gallyas silver stain (see Fig. 2x), suggesting the presence of both pretangles and NFTs in the brains of $2\times TgTau^{+/-}APP^{+/-}$ mice at 23 months of age. Phenotypic variations were also recognized in both $2\times TgTau^{+/-}APP^{+/-}$and $1\times TgTau^{+/-}APP^{-/-}$ like those in TgTauP301L.

Aβ core plaques labeled by Ab9201 appeared from 8 months of age in both $2\times TgTau^{+/-}APP^{+/-}$ and $1\times TgTau^{-/-}APP^{+/-}$. Numbers and distributions were increased with age in both groups. However, there were no differences in the initiation and distribution of Aβ deposits between $2\times TgTau^{+/-}APP^{+/-}$ (Fig. 1q–t) and $1\times TgTau^{-/-}APP^{+/-}$ (Fig. 1u–x). Furthermore, there were no differences in diffuse Aβ plaques at 16–23 months of age in the two group. From 8 months of age, dystrophic neurites around Aβ cores were present (Fig. 2a). The appearance of phosphorylated tau deposits in dystrophic neurites was enhanced in $2\times TgTau^{+/-}APP^{+/-}$ (Fig. 2c) compared with that in $1\times TgTau^{+/-}APP^{-/-}$ (Fig. 2d). These findings suggested that tauopathy does not induce Aβ amyloidosis, but rather Aβ amyloidosis accelerates phosphorylation and tangle formation of accumulated tau.

Then, phosphorylated tau was examined in detail in the brain of a 23-month-old $2\times TgTau^{+/-}APP^{+/-}$ mouse (Fig. 2e,g,h). Numerous neuropil threads were detected by AT8 staining in the cerebral cortex of the brain (Fig. 2g). There were phosphorylated tau-positive, Gallyas silver stain-negative neurites in the cerebral white matter (Fig. 2h), suggesting the presence of pretangles in the neuronal process. There was no apparent correlation between Aβ amyloid cores and NFTs, as shown in Figure 2i,j. Enhanced GSK-3β staining was also observed (Fig. 2k).

Neurons containing phosphorylated tau-positive pretangles were significantly enhanced and 3.7 times more frequently in the $2\times TgTau^{+/-}APP^{+/-}$ (63%, 5/8) compared with $1\times TgTau^{+/-}APP^{-/-}$ (17%, 5/29) at 23 months of age (Table I, $P = 0.0107$: χ^2 test; Graph Pad Prism 5). Glial tangles were also prominent in the brains of $2\times TgTau^{+/-}APP^{+/-}$: 6/8 (75%) of $2\times TgTau^{+/-}APP^{+/-}$ and 11/29 (38%) of $1\times TgTau^{+/-}APP^{-/-}$ mice ($P = 0.06$). However, there was no significant difference in the incidence of GFTs. Thus, Aβ enhances pretangle formation in neurons and processes.

These pretangles were labeled by antibodies against special phosphorylation sites at serine199 (Fig. 2r), at serine202 (Fig. 2s), at serine202/threonine205 (Fig. 2t), at threonine231/serine235 (Fig. 2u), at serine396/serine404 (Fig. 2v), and at serine413 (Fig. 2w), with conformational changes by MC1 (Fig. 2q) and by Gallyas silver staining (Fig. 2x). These findings correspond to those detected in TgTauP301L and patients with Alzheimer's disease or FTDP-17, suggesting that the appearance, severity, and modifications of accumulated tau are more accelerated by Aβ amyloidosis in $2\times TgTau^{+/-}APP^{+/-}$ than in $1\times TgTau^{+/-}APP^{-/-}$ mice.

To confirm the enhancement and acceleration of tau phosphorylation and NFTs formation, we examined the presence and amounts of sarkosyl-insoluble phosphorylated tau in the $2\times TgTau^{+/-}APP^{+/-}$ and $1\times TgTau^{+/-}APP^{-/-}$ 23-month-old mice by Western blot (Fig. 3). In the first Tris buffer-soluble fractions, human-specific tau antibody HT7 labeled the 66-kD bands. TAU-5 demonstrated 66-kD and 55-kD bands. There were no significant differences in the amounts of human and mouse tau in the Tris-soluble brain fractions of the two groups (Fig. 3a). Almost equal amounts of

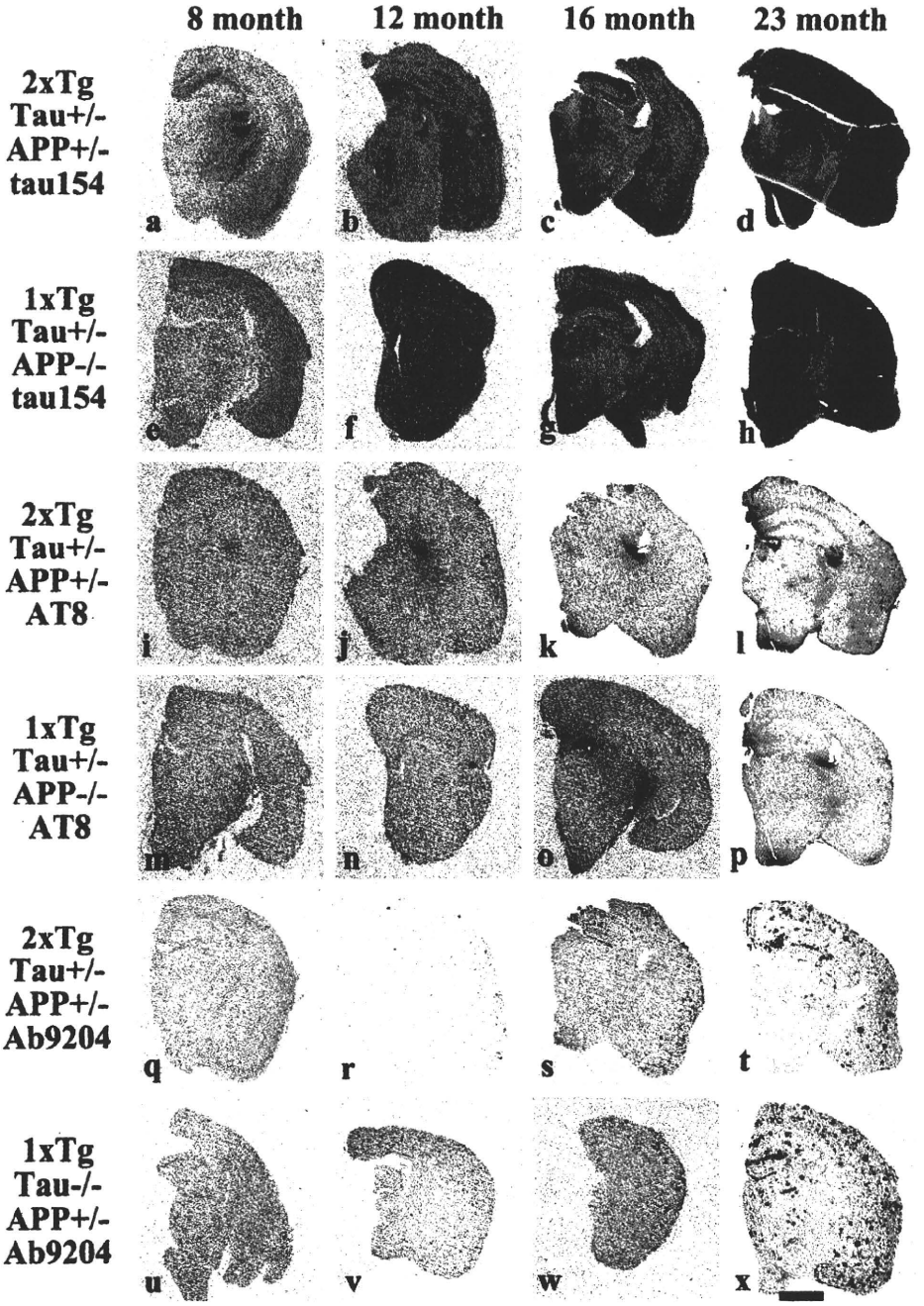

Fig. 1. Time course of accumulation of human tau, phosphorylated tau, and Aβ in 8–23-month-old $2\times TgTau^{+/-}APP^{+/-}$ (**a–d,i–l,q–t**), $1\times Tau^{+/-}APP^{-/-}$ (**e–h,m–p**), and $1\times TgTau^{-/-}APP^{+/-}$ (**u–x**) mice. Mouse sections were stained with tau154 that specifically detects human tau, AT8 for phosphorylated tau at serine202/threonine205, and Ab9204 for Aβ. Scale bar = 800 μm. [Color figure can be viewed in the online issue, which is available at wileyonlinelibrary.com.]

human tau were detected in the sarcosyl-soluble fractions from the brains of both groups (Fig. 3b). However, increased amounts of 66-kD full-length human tauP301L and their 58-kD fragments were increased in the sarkosyl-insoluble brain fraction of $2\times TgTau^{+/-}APP^{+/-}$ compared with those of $1\times TgTau^{+/-}APP^{-/-}$. These

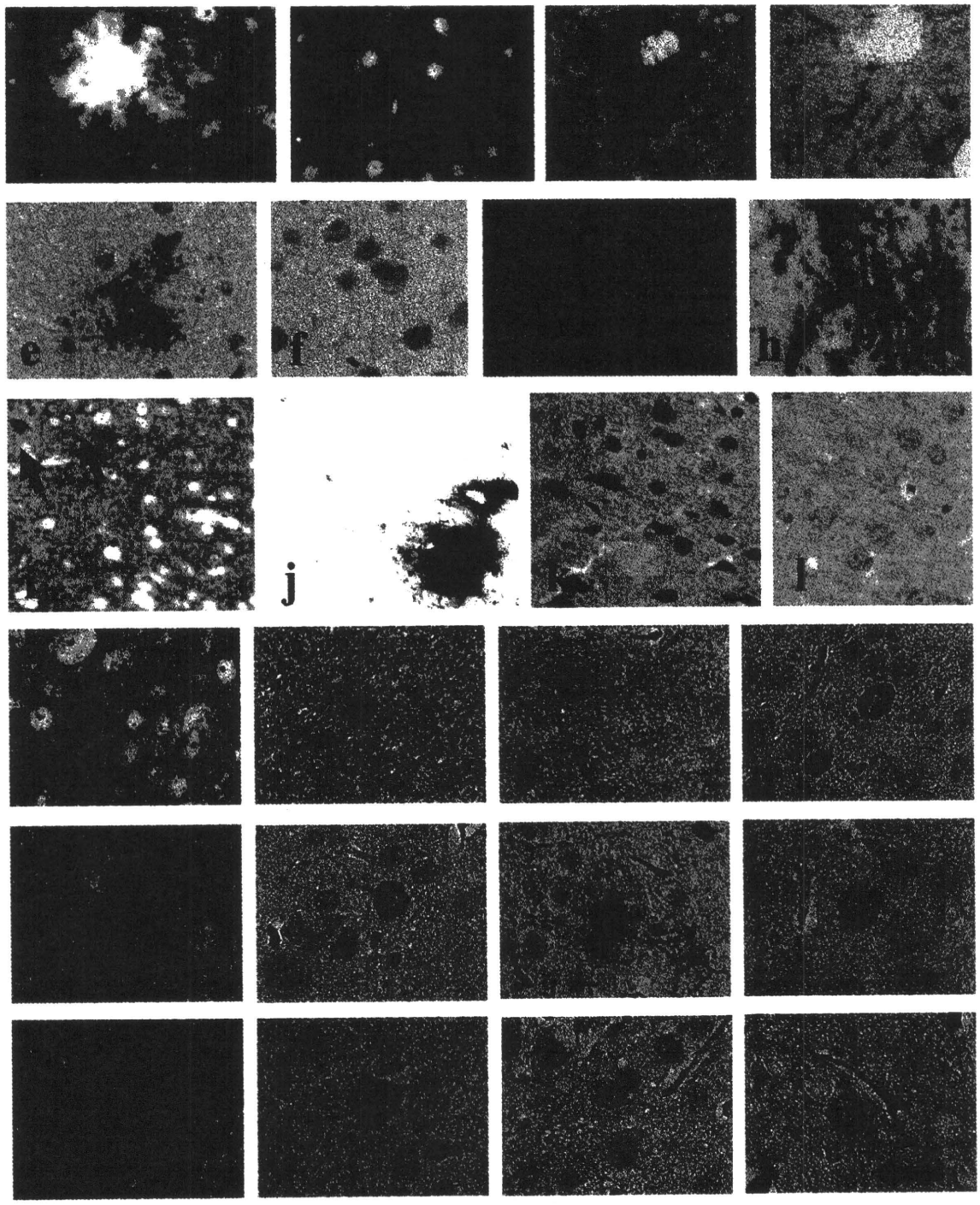

Fig. 2. Immunostaining of $2\times TgTau^{+/-}APP^{+/-}$ (**a,c,e,g–k,m–x**), $1\times TgTau^{+/-}APP^{-/-}$ (**b,f,l**), and $1\times TgTau^{-/-}APP^{+/-}$ (**d**) mice. Sections were stained with tau154 (a,b,i), AT8 (c–h), Ab9204 (j), anti-GSK3β (k,l). Cerebral cortex of $2\times TgTau^{+/-}APP^{+/-}$ was stained anti-tau antibodies; tau-154 (m), HT7 (n), CP27 (o), TAU-5 (p), MC1 (q), anti-PS199 (r), CP13 (s), AT8 (t), anti-PT231/PS235 (u), PHF1 (v), anti-PS413 (w), and Gallyas-Braak stain (x). Scale bar = 12.5 μm. [Color figure can be viewed in the online issue, which is available at wileyonlinelibrary.com.]

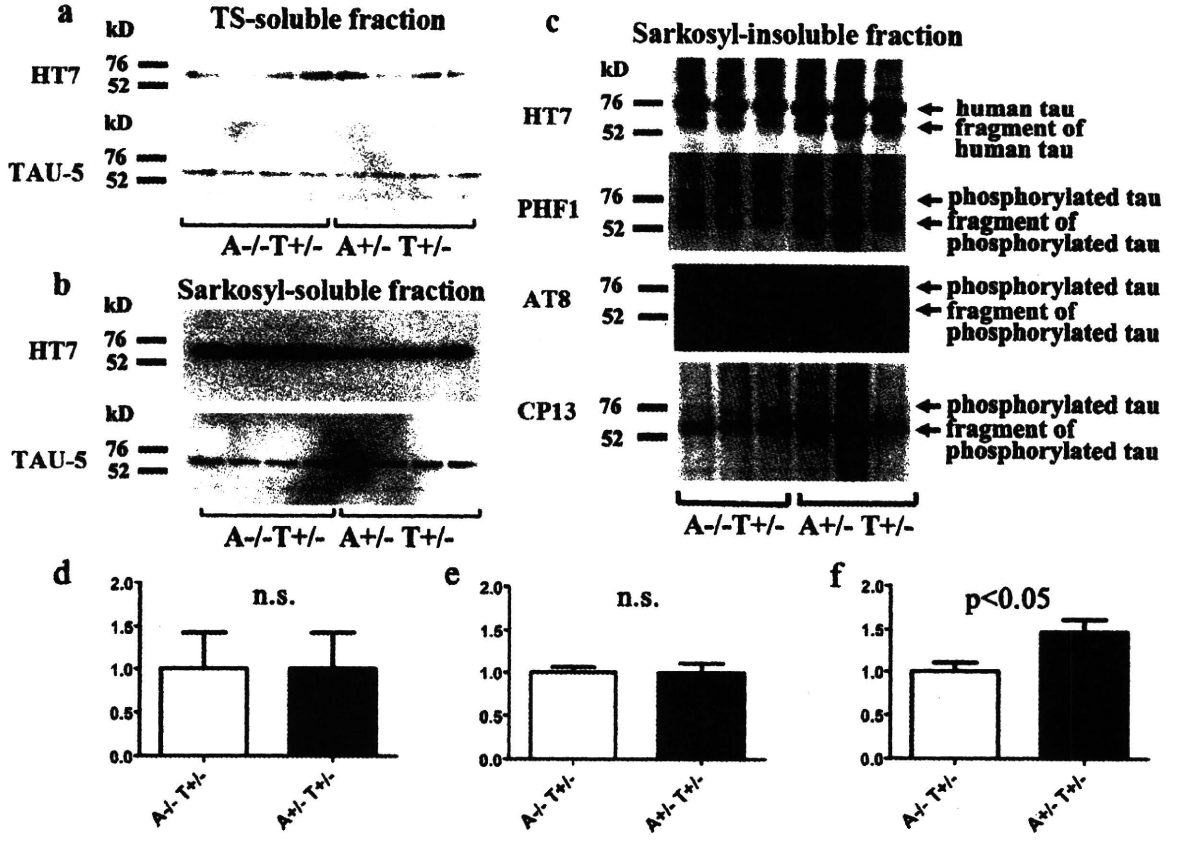

Fig. 3. Western blotting of brain extracts from $2\times TgTau^{+/-}APP^{+/-}$ ($A^{+/-}T^{+/-}$) and $1\times TgTau^{+/-}APP^{-/-}$ ($A^{-/-}T^{+/-}$). **a:** TS-soluble fraction stained with HT7 and TAU-5. **b:** Sarkosyl-soluble fraction stained with HT7 and TAU-5. **c:** Sarcosyl-insoluble fraction stained with HT7, PHF-1, AT8, and CP13. The signal intensity of tau in the sarkosyl-insoluble fraction (**f**) was significantly increased in $2\times TgTau^{+/-}APP^{+/-}$ compared with that in $1\times TgTau^{+/-}APP^{-/-}$; however, that in the TS-soluble fraction (**d**) and sarkosyl-soluble fraction (**e**) did not differ. The mean intensity of the band in $1\times TgTau^{+/-}APP^{-/-}$ is shown as 1.

TABLE I. NFTs and GFTs in $2\times TgTau^{+/-}APP^{+/-}$ and $1\times TgTau^{+/-}APP^{-/-}$

Genotype	$2\times TgTau^{+/-}APP^{+/-}$	$1\times TgTau^{+/-}APP^{-/-}$
Neurofibrillary pretangles	63% (5/8)**	17% (5/29)
Glial fibrillary pretangles	75% (6/8)	38% (11/29)

**$P = 0.0107$.

increased tau isoforms were also labeled by antibody PHF1, AT8, and CP13, suggesting that sarkosyl-insoluble tau is hyperphosphorylated and conformationally changed in the most insoluble brain fractions, which corresponds to those recognized in Alzheimer's disease brains (Fig. 3c). Thus, acceleration of tauopathy in the $2\times TgTau^{+/-}APP^{+/-}$ brain was also detected by biochemical examinations.

DISCUSSION

Both $2\times TgTau^{+/-}APP^{+/-}$ and $1\times TgTau^{+/-}APP^{-/-}$ showed initiation and accumulation of tauP301L starting at 3 months, and those accumulations progressively spread from the hippocampus to the cortices, amygdala, and brainstem. The initial appearance of dystrophic neurites around the core plaques was detected in both mice at the same period of 8 months of age. The number and size of phosphorylated tau were enhanced in dystrophic neurites of $2\times TgTau^{+/-}APP^{+/-}$ mice. Phosphorylated tau-positive pretangles, NFTs, and GFTs and phenotypic variation were also reproduced in both mice. However, the prevalence of mice exhibiting pretangles, NFTs, and phosphorylated tau-positive neuropils was significantly increased in $2\times TgTau^{+/-}APP^{+/-}$ compared with $1\times TgTau^{+/-}APP^{-/-}$ mice at 23 months of age. The distributions of pretangles and NFTs were not correlated with the presence of core plaques. These findings suggest that the presence of Aβ amyloidosis partially enhances the accumulation of phosphorylated tau in neurons and neuronal processes.

Subsequent generation of Aβ plaques and tangles and neurodegeneration have been exhibited by regulatory expression model mice of tauP301L (rTg4510; Spires et al., 2006; Spires-Jones et al., 2008; de Calington et al., 2009) and APPNL1 (rTg3696AB; Paulson et al., 2008). In our $2\times TgTau^{+/-}APP^{+/-}$ mice, however, the appearances of pretangles, NFTs, and GFTs were markedly delayed at 23 months of age. Tauopathy was detected at 18 months of age in TgtauP301L, so about a 5-month delay was observed. Florid pathology including brain atrophy, neuronal cell loss, and gliosis detected in TgtauP301L was milder in both $2\times TgTau^{+/-}APP^{+/-}$ and $1\times TgTau^{+/-}APP^{-/-}$ even at 23 months of age. This delay and a milder form of tau pathology were observed in $1\times TgTau^{+/-}APP^{-/-}$, so one possible explanation is that alteration of the genetic background by crossing strains from FBV in TgTauP301L with FVB/B6/SJL occurred in the crossing of double heterozygotes Tg. For this reason, we analyzed many heterozygotes of mice in this study to confirm this phenomenon statistically and to show significant enhancement of tau pathology by Aβ in $2\times TgTau^{+/-}APP^{+/-}$.

Development of Aβ burden was completely identical among $2\times TgTau^{+/-}APP^{+/-}$, $1\times TgTau^{-/-}APP^{+/-}$, and Tg2576. Initial Aβ deposits were detected at 8 months of age, and there was no significant difference in the progressive distribution and density among these three strains. In other double and triple Tg mice, genetically augmented tau levels and hyperphosphorylation in the 3×Tg-AD did not show any effect on the onset and progression of Aβ pathology (Oddo et al., 2007). The somatodendritic tau accumulation is dependent on parenchymal Aβ deposits (Oddo et al., 2009). Aβ-dependent triosephosphate isomerase nitrotyrosination induces glycation and tau fibrillation (Guix et al., 2009). Thus, unidirectional facilitation of tauopathy by Aβ amyloidosis and Aβ oligomer was considered (Oddo et al., 2006b). The initial alteration of Tg2576 brain was Aβ dimers in lipid rafts at 6 months of age, and subsequent accumulation of phosphorylated tau was identified (Kawarabayashi et al., 2004). Because enhancement of pretangles, NFTs and GTFs appeared in the late stage of Aβ burden consisting of many core plaques and diffuse plaques, the acceleration effect of tauopathy by Aβ amyloid is not considered very strong, but the incubation period seems to be long despite previous findings regarding the mutant presenilin-1 effect on APP double Tg mice (Holcomb et al., 1998).

As clearly shown in TgtauP301L, many tau transgenic mice exhibited loss of neurons and synapses. Accumulation of tau in axonal defects was an early event in the brains of AD and APP Tg mice (Stokin et al., 2005). Suppression of tau expression in mice expressing a repressible tauP301L developing progressive NFTs, neuronal cell loss, and behavioral impairments recovered memory function and neuron numbers (Santacruz et al., 2005). Transgenic TAU zebrafish clearly showed that GSK3β-mediated NFT formation actually induces neuronal cell death (Paquet et al., 2009). Neurotoxicity induced by fibrillar Aβ on hippocampal cultured neurons is mediated by tau (Rapoport et al., 2002). There was no neuronal cell loss or synaptic losses at 23 months of age in $2\times TgTau^{+/-}APP^{+/-}$. These findings indicated that an NFT burden more severe than that shown in $2\times TgTau^{+/-}APP^{+/-}$ is necessary to induce neuronal cell loss and that Aβ amyloid fibrils and oligomer were not sufficient to induce this neurodegenerative processes.

Other double transgenic mice obtained by crossing Tg2576 and tau transgenic mice expressing tauG272V, P301L, and R406W showed an increase in tau phosphorylation at serine262 and -422 (Pérez et al., 2005). Lithium, a well-known drug that inhibits GSK-3 activities, reduced tau phosphorylation but did not alter the Aβ load (Caccamo et al., 2007). Injection of Aβ42 fibrils into the brains of tauP301L transgenic mice caused a fivefold increase in the number of NFTs in the amygdala where neurons projected to the injected site, 18 days after Aβ42 injection (Götz et al., 2001). Amyloid induces tauopathy through activation of GSK-3β in APP-V717I × TauP301L mice (Terwel et al., 2008). Tau reduction can block Aβ and excitotoxin-induced neuronal dysfunction (Robertson et al., 2007). All these findings indicate that Aβ might induce NFTs through phosphorylation of tau and formation of conformationally changed tau and GSK3β activation. In accordance with these findings, $2\times TgTau^{+/-}APP^{+/-}$ showed enhanced phosphorylation at serine199, at serine202, at serine202/threonine205, at threonine231/serine235, at serine 396/serine404, and at serine413 and the presence of conformational alteration and argylophilic properties as well as increased expression of GSK-3β. Biochemical analysis further confirmed the histological findings and indicated that this hyperphosphorylated and conformationally changed tau acutully gains insolubility, leading to accumulation of aggregated tau in the sarkosyl-insoluble fraction in the brain.

In summary, enhancement of tauopathy by Aβ may partially initiate pretangle formation in the neuronal processes and cytoplasm. Based on the presence of many pretangles in the cortex, NFTs and GFTs emerged. These findings correspond to conventional neuropathological findings and other reports on AD model mice (LaFerla and Oddo, 2005, Spires-Jones et al., 2009). Our data and these reports support the hypothesis that disturbance of axonal transport of phosphorylated tau in the axons is an early event induced by Aβ amyloid deposition. Further drug development targeting this step would be desirable.

ACKNOWLEDGMENTS

We thank K. Sato, M. Ono, K. Iinuma, Y. Sato, R. Tushima, and I. Shirahama for technical assistance; Dr. TC Saido for generously donating Ab9204; Dr. Peter Davies for CP27, CP13, MC1, and PHF-1 antibodies; and Dr. Koich Ishiguro for tau-154, PS199, anti-PT231/PS235, anti-PS413, anti-GSK3β antibodies.

REFERENCES

Caccamo A, Oddo S, Tran LX, LaFerla FM. 2007. Lithium reduces tau phosphorylation but not Aβ or working memory deficits in a transgenic model with both plaques and tangles. Am J Pathol 170:1669–1675.

de Calignon A, Spires-Jones TL, Pitstick R, Carlson GA, Hyman BT. 2009. Tangle-bearing neurons survive despite disruption of membrane

integrity in a mouse model of tauopathy. J Neuropathol Exp Neurol 68:757–761.

Ghiso JA, Holton J, Miravalle L, Calero M, Lashley T, Vidal R, Houlden H, Wood N, Neubert TA, Rostagno A, Plant G, Revesz T, Frangione B. 2001. Systemic amyloid deposits in familial British dementia. J Biol Chem 276:43909–43914.

Götz J, Chen F, van Dorpe J, Nitsch RM. 2001. Formation of neurofibrillary tangles in P301L tau transgenic mice induced by Aβ42 fibrils. Science 293:1491–1495.

Guix FX, Ill-Raga G, Bravo R, Nakaya T, de Fabritiis G, Coma M, Miscione GP, Villà-Freixa J, Suzuki T, Fernàndez-Busquets X, Valverde MA, de Strooper B, Muñoz FJ. 2009. Amyloid-dependent triosephosphate isomerase nitrotyrosination induces glycation and tau fibrillation. Brain 132:1335–1345.

Hardy J. 2009. The amyloid hypothesis for Alzheimer's disease: a critical reappraisal. J Neurochem 110:1129–1134.

Holcomb L, Gordon MN, McGowan E, Yu X, Benkovic S, Jantzen P, Wright K, Saad I, Mueller R, Morgan D, Sanders S, Zehr C, O'Campo K, Hardy J, Prada CM, Eckman C, Younkin S, Hsiao K, Duff K. 1998. Accelerated Alzheimer-type phenotype in transgenic mice carrying both mutant amyloid precursor protein and presenilin 1 transgenes. Nat Med 4:97–100.

Holmes C, Boche D, Wilkinson D, Yadegarfar G, Hopkins V, Bayer A, Jones RW, Bullock R, Love S, Neal JW, Zotova E, Nicoll JA. 2008. Long-term effects of Aβ42 immunization in Alzheimer's disease: follow-up of a randomised, placebo-controlled phase I trial. Lancet 372:216–223.

Hutton M, Lendon CL, Rizzu P, Baker M, Froelich S, Houlden H, Pickering-Brown S, Chakraverty S, Isaacs A, Grover A, Hackett J, Adamson J, Lincoln S, Dickson D, Davies P, Petersen RC, Stevens M, de Graaff E, Wauters E, van Baren J, Hillebrand M, Joosse M, Kwon JM, Nowotny P, Che LK, Norton J, Morris JC, Reed LA, Trojanowski J, Basun H, Lannfelt L, Neystat M, Fahn S, Dark F, Tannenberg T, Dodd PR, Hayward N, Kwok JB, Schofield PR, Andreadis A, Snowden J, Craufurd D, Neary D, Owen F, Oostra BA, Hardy J, Goate A, van Swieten J, Mann D, Lynch T, Heutink P. 1998. Association of missense and 5′-splice-site mutations in tau with the inherited dementia FTDP-17. Nature 393:702–705.

Kawarabayashi T, Shoji M, Younkin LH, Wen-Lang L, Dickson DW, Murakami T, Matsubara E, Abe K, Ashe KH, Younkin SG. 2004. Dimeric amyloid β protein rapidly accumulates in lipid rafts followed by apolipoprotein E and phosphorylated tau accumulation in the Tg2576 mouse model of Alzheimer's disease. J Neurosci 24:3801–3809.

LaFerla FM, Oddo S. 2005. Alzheimer's disease: Aβ, tau and synaptic dysfunction. Trends Mol Med 11:170–176.

Lewis J, Dickson DW, Lin WL, Chisholm L, Corral A, Jones G, Yen SH, Sahara N, Skipper L, Yager D, Eckman C, Hardy J, Hutton M, McGowan E. 2001. Enhanced neurofibrillary degeneration in transgenic mice expressing mutant tau and APP. Science 293:1487–1491.

Love S, Bridges LR, Case CP. 1995. Neurofibrillary tangles in Niemann-Pick disease type C. Brain 118:119–129.

Murakami T, Paitel E, Kawarabayashi T, Ikeda M, Chishti MA, Janus C, Matsubara E, Sasaki A, Kawarai T, Phinney AL, Harigaya Y, Horne P, Egashira N, Mishima K, Hanna A, Yang J, Iwasaki ,K, Takahashi M, Fujiwara M, Ishiguro K, Bergeron C, Carlson GA, Abe K, Westaway D, St. George-Hyslop P, Shoji M. 2006. Cortical neuronal and glial pathology in TgTauP301L transgenic mice: neuronal degeneration, memory disturbance, and phenotypic variation, Am J Pathol 169:1365–1375.

Oddo S, Billings L, Kesslak JP, Cribbs DH, LaFerla FM. 2004. Aβ immunotherapy leads to clearance of early, but not late, hyperphosphorylated tau aggregates via the proteasome. Neuron 43:321–332.

Oddo S, Vasilevko V, Caccamo A, Kitazawa M, Cribbs DH, LaFerla FM. 2006a. Reduction of soluble Aβ and tau, but not soluble Aβ alone, ameliorates cognitive decline in transgenic mice with plaques and tangles. J Biol Chem 281:39413–39423.

Oddo S, Caccamo A, Tran L, Lambert MP, Glabe CG, Klein WL, LaFerla FM. 2006b. Temporal profile of amyloid-β (Aβ) oligomerization in an in vivo model of Alzheimer disease. A link between Aβ and tau pathology. J Biol Chem 281:1599–1604.

Oddo S, Caccamo A, Cheng D, Jouleh B, Torp R, LaFerla FM. 2007. Genetically augmenting tau levels does not modulate the onset or progression of Aβ pathology in transgenic mice. J Neurochem 102:1053–1063.

Oddo S, Caccamo A, Tseng B, Cheng D, Vasilevko V, Cribbs DH, LaFerla FM. 2008. Blocking Aβ42 accumulation delays the onset and progression of tau pathology via the C terminus of heat shock protein70-interacting protein: a mechanistic link between Aβ and tau pathology. J Neurosci 28:12163–12175.

Oddo S, Caccamo A, Cheng D, LaFerla FM. 2009. Genetically altering Aβ distribution from the brain to the vasculature ameliorates tau pathology. Brain Pathol 19:421–430.

Paquet D, Bhat R, Sydow A, Mandelkow EM, Berg S, Hellberg S, Fälting J, Distel M, Köster RW, Schmid B, Haass C. 2009. A zebrafish model of tauopathy allows in vivo imaging of neuronal cell death and drug evaluation. J Clin Invest 119:1382–1395.

Paulson JB, Ramsden M, Forster C, Sherman MA, McGowan E, Ashe KH. 2008. Amyloid plaque and neurofibrillary tangle pathology in a regulatable mouse model of Alzheimer's disease. Am J Pathol 173:762–772.

Pérez M, Ribe E, Rubio A, Lim F, Morán MA, Ramos PG, Ferrer I, Isla MT, Avila J. 2005. Characterization of a double (amyloid precursor protein-tau) transgenic: tau phosphorylation and aggregation. Neuroscience 130:339–347.

Rapoport M, Dawson HN, Binder LI, Vitek MP, Ferreira A. 2002. Tau is essential to β-amyloid-induced neurotoxicity. Proc Natl Acad Sci U S A 99:6364–6369.

Roberson ED, Scearce-Levie K, Palop JJ, Yan F, Cheng IH, Wu T, Gerstein H, Yu GQ, Mucke L. 2007. Reducing endogenous tau ameliorates amyloid β-induced deficits in an Alzheimer's disease mouse model. Science 316:750–754.

Santacruz K, Lewis J, Spires T, Paulson J, Kotilinek L, Ingelsson M, Guimaraes A, DeTure M, Ramsden M, McGowan E, Forster C, Yue M, Orne J, Janus C, Mariash A, Kuskowski M, Hyman B, Hutton M, Ashe KH. 2005. Tau suppression in a neurodegenerative mouse model improves memory function. Science 309:476–481.

Spires TL, Orne JD, SantaCruz K, Pitstick R, Carlson GA, Ashe KH, Hyman BT. 2006. Region-specific dissociation of neuronal loss and neurofibrillary pathology in a mouse model of tauopathy. Am J Pathol 168:1598–1607.

Spires-Jones TL, de Calignon A, Matsui T, Zehr C, Pitstick R, Wu HY, Osetek JD, Jones PB, Bacskai BJ, Feany MB, Carlson GA, Ashe KH, Lewis J, Hyman BT. 2008. In vivo imaging reveals dissociation between caspase activation and acute neuronal death in tangle-bearing neurons. J Neurosci 28:862–867.

Spires-Jones TL, Stoothoff WH, de Calignon A, Jones PB, Hyman BT. 2009. Tau pathophysiology in neurodegeneration: a tangled issue. Trends Neurosci 32:150–159.

Stokin GB, Lillo C, Falzone TL, Brusch RG, Rockenstein E, Mount SL, Raman R, Davies P, Masliah E, Williams DS, Goldstein LS. 2005. Axonopathy and transport deficits early in the pathogenesis of Alzheimer's disease. Science 307:1282–1288.

Terwel D, Muyllaert D, Dewachter I, Borghgraef P, Croes S, Devijver H, Van Leuven F. 2008. Amyloid activates GSK-3β to aggravate neuronal tauopathy in bigenic mice. Am J Pathol 172:786–798.

Tomidokoro Y, Ishiguro K, Harigaya Y, Matsubara E, Ikeda M, Park JM, Yasutake K, Kawarabayashi T, Okamoto K, Shoji M. 2001. Aβ amyloidosis induces the initial stage of tau accumulation in APP(Sw) mice. Neurosci Lett 299:169–172.

Journal of Neuroscience Research

Journal of Neuroscience Research 89:576–584 (2011)

Factors Responsible for Neurofibrillary Tangles and Neuronal Cell Losses in Tauopathy

Yasuhito Wakasaya,[1] Takeshi Kawarabayashi,[1]* Mitsunori Watanabe,[1] Yukiko Yamamoto-Watanabe,[1] Ayumi Takamura,[1] Tomoko Kurata,[2] Tetsuro Murakami,[2] Koji Abe,[2] Kiyofumi Yamada,[3] Koichi Wakabayashi,[4] Atsushi Sasaki,[5] David Westaway,[6] Peter St. George Hyslop,[7] Etsuro Matsubara,[1] and Mikio Shoji[1]

[1]Department of Neurology, Institute of Brain Science, Hirosaki University Graduate School of Medicine, Hirosaki, Japan
[2]Department of Neurology, Okayama University Graduate School of Medicine, Dentistry and Pharmaceutical Sciences, Okayama, Japan
[3]Department of Neuropsychopharmacology and Hospital Pharmacy, Nagoya University Graduate School of Medicine, Nagoya, Japan
[4]Department of Neuropathology, Institute of Brain Science, Hirosaki University Graduate School of Medicine, Hirosaki, Japan
[5]Department of Pathology, Saitama Medical University, Saitama, Japan
[6]Centre for Prions and Protein Folding Diseases, 204 Environmental Engineering Building, University of Alberta, Edmonton, Alberta, Canada
[7]Centre for Research in Neurodegenerative Diseases, Departments of Medicine (Neurology) and Laboratory Medicine and Pathobiology, University of Toronto, Toronto, Ontario, Canada

TgTauP301L mice that overexpress the mutant human tauP301L present in FTDP-17 reproduce neurofibrillary tangles (NFTs), neuronal cell losses, memory disturbance, and substantial phenotypic variation. To demonstrate factors responsible for NFT formation and neuronal cell losses, sets of TgTauP301L for comparison with or without NFTs and neuronal cell losses were studied with oligonucleotide microarrays. Gene expressions were altered in biological pathways, including oxidative stress, apoptosis, mitochondrial fatty acid betaoxidation, inflammatory response pathway, and complement and coagulation cascade pathways. Among 24 altered genes, increased levels of apolipoprotein D (ApoD) and neuronal PAS domain protein 4 (Npas4) and decreased levels of doublecortin (DCX) and potassium channel, voltage-gated, shaker-related subfamily, β member 1 (Kcnab1) were found in the TgTauP301L with NFTs and neuronal cell losses, Alzheimer's brains, and tauopathy brains. Thus, many biological pathways and novel molecules are associated with NFT formation and neuronal cell losses in tauopathy brains.

Key words: tauopathy; Apo D; Npas4; DCX; Kcnab1

Alzheimer's disease (AD) brains are invariably characterized by two pathological features: initial Aβ amyloidosis by extracellular deposition of Aβ, and subsequent tauopathy with intracellular accumulation of neurofibrillary tangles (NFTs) comprising abnormal aggregates of phosphorylated tau. Aβ cascade from Aβ deposits to the final appearance of NFTs and neuronal cell losses is the major hypothesis that explains all steps in the pathogenesis of AD (Hardy, 2009). Although soluble Aβ oligomers are cardinal molecules that adversely affect synaptic structures and plasticity, leading to memory disturbance, neuronal cell loss is closely related to the presence of NFTs (Spires-Jones et al., 2009). Accumulation of tau in axonal defects is an early event in AD brain and in APP transgenic mouse (Stokin et al., 2005). Suppression of tau expression in mice expressing a repressible tauP301L and developing progressive NFTs, neuronal cell losses, and behavior

Contract grant sponsor: Ministry of Health, Labor and Welfare of Japan (to M.S.); Contract grant sponsor: Ministry of Education, Culture, Sports, Science and Technology, Japan; Contract grant number: 19390233 (to M.S.); Contract grant number: 19590976 (to T.K.); Contract grant number: 18590968 (to E.M.); Contract grant sponsor: The Mochida Memorial Foundation for Medical and Pharmaceutical Research (to M.W.); Contract grant sponsor: Hirosaki University Institutional Research (to M.S.).

*Correspondence to: Dr. Takeshi Kawarabayashi, Department of Neurology, Institute of Brain Science, Hirosaki University Graduate School of Medicine, 5 Zaifucho, Hirosaki 036-8562, Japan.
E-mail: tkawara@cc.hirosaki-u.ac.jp

Received 1 September 2010; Revised 8 November 2010; Accepted 9 November 2010

Published online 13 January 2011 in Wiley Online Library (wileyonlinelibrary.com). DOI: 10.1002/jnr.22572

impairments recovered memory function and neuron numbers (Santacruz et al., 2005). However, once NFTs are formed, these features are irreversible (Holmes et al., 2008). Transgenic tau zebrafish have clearly shown that GSK3β-mediated NFT formation actually induces neuronal cell losses (Paquet et al., 2009). These findings support the hypothesis that tauopathy is the critical event in neuronal cell losses in AD and frontotemporal dementia (FTD) patients. In FTD and parkinsonism linked to chromosome 17 (FTDP-17), there is large variation in the clinical and neuropathological features of disease among patients showing the same mutation within a family. We recently established a tauopathy model mouse expressing 2N4R human tauP301L, developing florid pathology, including numerous pretangles, NFTs, glial fibrillary tangles (GFTs), gliosis, and neuronal cell losses in the frontotemporal areas of the cerebrum accompanied by cerebral atrophy (TgTauP301L; Murakami et al., 2006). As expected, TgTauP301L also showed variation in phenotypic manifestation. Given that the genetic modifiers or associated molecules are clarified by comparison between individuals showing severe pathology including numerous NFTs and neuronal cell losses and those with only pretangles, study of the variance both in families with FTDP-17 and in our mouse model can contribute to clarifying the pathological cascade from accumulation of phosphorylated tau to NFT formation and final neuronal cell losses. On the basis of this hypothesis, here we analyzed oligonucleotide microarrays to determine the mRNA expression profile in TgTauP301L with and without tau pathology and showed the alterations of biological pathways and novel proteins associated with NFTs and neuronal cell losses.

MATERIALS AND METHODS

Subjects

TgTauP301L were back-crossed to FVB/N strain mice for more than six generations to obtain a uniform genetic background. Two sets of TgTauP301L consisted of the 517 mouse with human tau accumulation (Fig. 1Ba–e) and the 512 mouse showing extensive NFTs and neuronal cell losses (Fig. 1Bf–j), which were compared at 24 months of age, as well as the 739 mouse with only human tau accumulation (Fig. 1Aa,b, Bk–o) and the 736 mouse showing extensive NFTs and neuronal cell losses (Fig. 1Ac,d, Bp–t), which were compared at 26 months of age, using oligonucleotide microarrays. After mice were sacrificed under ether anesthesia, the sagittal half of the brain was immediately frozen at −80°C for Western blot and microarray analysis, and the other half of the brain was analyzed histologically. An additional 185 TgTauP301L between 3 months and 30 months of age, 52 nontransgenic control littermates (3–30 months old), and autopsy brains from five patients with Alzheimer's disease (ages 65–81 years), five patients with tauopathy [two frontotemporal dementia (FTD), two corticobasal degeneration, and one supranuclear palsy (ages 71–78 years)], and five normal controls (ages 71–91 years) were examined by immunostaining and biochemical analysis.

Target RNA Preparation and Oligonucleotide Array Expression Analysis

Total RNAs from two sets of mouse brains were isolated using the Trizol reagent (Invitrogen, Carlsbad, CA) and purified with a RNeasy Mini Kit (Qiagen, Valencia, CA). The One-Cycle cDNA synthesis kit from Affymetrix was used to synthesize cDNA from 2 μg of total RNA. Biotinylated cRNA was generated from the cDNA using the IVT Labeling Kit (Affymetrix, Santa Clara, CA), followed by fragmentation of the cRNA target using a fragmentation buffer for 35 min at 94°C before chip hybridization, then 15 μg of fragmented cRNA was added to a hybridization cocktail (0.05 μg/μl fragmented cRNA, 50 pM control oligonucleotide B2, 1.5 pM *BioB*, 5 pM *BioC*, 25 pM *BioD*, and 100 pM *cre* hybridization controls, 0.1 mg/ml herring sperm DNA, 0.5 mg/ml acetylated BSA, 100 mM MES, 1 M Na^+, 20 mM EDTA, 0.01%/Tween 20). Ten micrograms of cRNA from each sample was hybridized to a separate oligonucleotide array (Affymetrix Mouse Genome 430 2.0) for 16 hr at 45°C in the GeneChip Hybridization Oven 640. The arrays were washed and stained with streptavidin phycoerythrin in the GeneChip Fluidics Station 450. Then, the arrays were scanned with a GeneChip Scanner 3000.

Data Analysis

The Affymetrix GeneChip Microarray Suite 5.0 (MAS5) algorithm was used to generate signal values and detection calls (present, absent or marginal). Only genes that had a "present" or "marginal" detection call on all four chips were chosen, with 24,330 identified for further analysis from a total of 45,101 genes. Ratios of changes in gene expression were obtained by the differences between 517 and 512 and between 739 and 736. Gene expression ratios of ≥ 2 or ≤ 0.5 were chosen as cutoff values, defining increased and decreased expression, respectively. Filtered genes identified as differentially expressed by twofold or greater in both comparisons were tested for statistical significance using moderated *t* statistics by the empirical Bayes method in the R package "limma" (Smyth, 2004). For moderated *t*-test, we choose a threshold of $P < 0.05$. The corresponding false-discovery rate was 0.076, meaning that 7.6% of the genes selected by this *P* value could be false-positive (Benjamini and Hochberg, 1995).

For biological interpretation of the differentially expressed genes, the number of appearances of each gene ontology (GO) term (http://www.geneontology.org/) was counted from each list of genes. Fisher's exact test to assess the significance for enrichment of genes within three kinds of GO categories (BP, biological process; MF, molecular function; CC, cellular component) in a list was performed by the GO Browser tool in GeneSpring GX 7.3.1 (Agilent Technologies, Santa Clara, CA).

We also performed a pathway analysis with parametric analysis of gene-set enrichment (PAGE; Kim and Volsky, 2005) to analyze the differential expression of predefined gene sets rather than individual genes. This test was implemented by calculating a Z score for a given gene set that measures the deviation of the average log-ratio for genes in the category

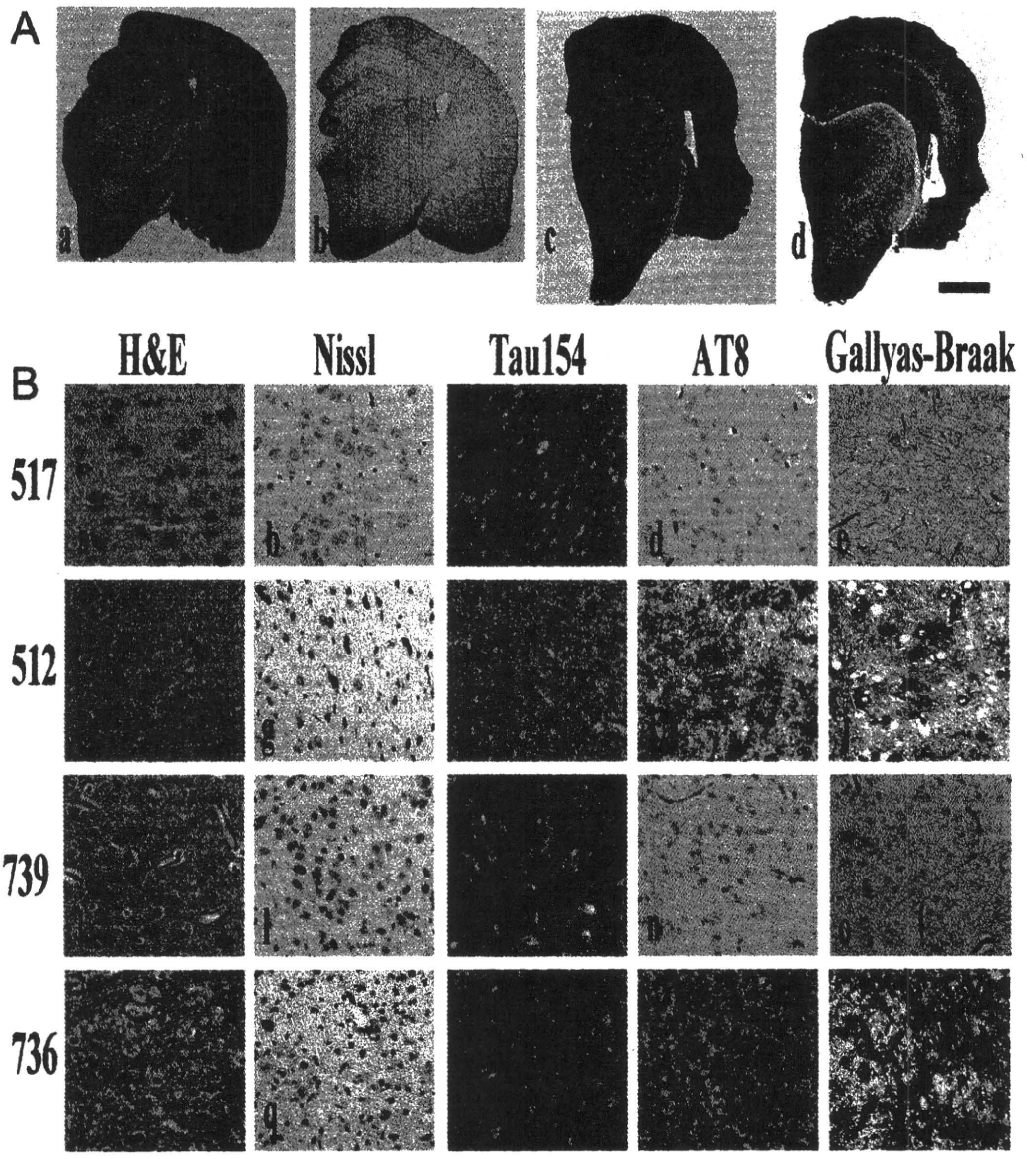

Fig. 1. Phenotypic variation in TgTauP301L mice. **A**: Brains of 739 (a,b) and 736 (c,d); a and c show tau154 staining, and b and d show Gallyas-Braak silver staining. Accumulation of human tauP301L was similar between 739 and 736. However, severe NFTs and brain atrophy were prominent in 736 (d). **B**: Brain sections of 517, 512, 739, and 736 were stained with hematoxylin and eosin (H&E; a,f,k,p), Nissl (b,g,l,q), tau154 antibody (c,h,m,r), AT8 antibody (d,i,n,s), and Gallyas-Braak silver staining (e,j,o,t). Neuronal cell losses and NFT formation were prominent in 512 (g,j) and 736 (q,t). Scale bar = 1 mm in A; 50 μm in B. [Color figure can be viewed in the online issue, which is available at wileyonlinelibrary.com.]

from the genome-wide average, in units of the standard deviation. The Z score for each category was calculated as

$$Z = (\bar{X} - \mu)\sigma/\sqrt{n},$$

where μ and σ represent the mean and the standard deviation of total -fold change values of genes after filtering by MAS5 detection call, respectively. $\bar{X}$ is the mean of -fold change values of genes for a given set, and n is the size of a given gene set. The predefined gene sets were created from GenMAPP (http://www.genmapp.org/).

Immunostaining

Tissues were fixed in 4% paraformaldehyde with 0.1 M phosphate buffer (pH 7.6) for 8 hr and embedded in paraffin. Five-micrometer-thick sections were prepared for immuno-

staining and Gallyas-Braak silver stain. For tau immunostaining, sections were immersed in 0.5% periodic acid for blocking intrinsic peroxidase and treated with 99% formic acid for 3 min. After blocking with 5% normal goat or horse serum, sections were incubated overnight with primary antibodies. The specific labeling was visualized using Vectastain Elite ABC kit (Vector, Burlingame, CA). Tissue sections were counterstained with hematoxylin. The following antibodies were used for immunostaining: tau154 (1:200), TAU-5 (1:1,000; Biosource. Camarillo, CA), AT8 (1:400; Innogenetics, Gent, Belgium; Murakami et al., 2006), antibodies to ApoD (1:1,000; Patel et al., 1995; 36C6, 1:100; Novocastra Laboratories, Newcastle, United Kingdom), antibodies to DCX (N-19, 1:200; C-18, 1:200; Santa Cruz Biotechnology, Santa Cruz, CA), antibody to Npas4 (1: 50, polyclonal antibody to purified Npas4; 1:100, NBP1-06574; Novus Biologicals, Littleton, CO), and antibody to Kcnab1 (1: 50; Santa Cruz Biotechnology).

Western Blotting

The remaining brain sample was homogenized in 9 volumes of Tris-saline buffer with protease inhibitors (Complete Inhibitor Cocktail tablets; Roche, Mannheim, Germany) and centrifuged at 55,000 rpm for 60 min at 4°C (TS buffer-soluble fraction). The pellet was homogenized again in 4 volumes of 1% sarkosyl in TS, incubated on ice for 30 min, and centrifuged at 55,000 rpm for 60 min at 4°C. The pellet was analyzed as the sarkosyl-insoluble fraction. The samples were boiled at 70°C in 4 volumes of SDS sample buffer, separated on 4–12% NuPAGE Bis-Tris Gel (Invitrogen, Carlsbad, CA), and the blots were labeled by antibodies. Signals were visualized with an enhanced chemiluminescence detection system (Pierce United Kingdom) and quantified by a luminoimage analyzer (LAS 1000-mini; Fuji Film, Tokyo, Japan). The signals were corrected by those of β-actin, and were tested for statistical significance using *t*-tests [TgTauP301L with NFTs and neuronal cell losses (n = 3) and without NFTs and neuronal cell losses (n = 3)]. All animal experiments were performed according to guidelines established in the *Guide for the care and use of laboratory animals* and by the ethical committee of Hirosaki University.

RESULTS

In comparing gene expression ratios between 517 and 512, 278 were increased and 162 were decreased. There were 477 increased gene expression ratios and 369 decreased gene expression ratios between 739 and 736. In the two comparisons of gene expression ratios, there were 52 up-regulations and 16 down-regulations in common. Among these 68 gene expressions, 37 gene expressions were significant, and 24 genes have already been described (Table I). There was no alteration of gene expression ratios for APP, MAPT, or GSK3β in 517, 512, 739, and 736 mouse brains.

According to biological pathways and gene expression groupings based on the GenMAPP database, comparison between 517 and 512 demonstrated seven down-regulated gene expression ratio groups. Five pathways consisted of up-regulated gene expression ratio groups. On comparison between 739 and 736, only one pathway showed a down-regulated gene expression group; however, 41 pathways showed up-regulated gene expression groups. Among these biological pathways, inflammatory response, mitochondrial fatty acid beta-oxidation, oxidative stress, apoptosis, and complement and coagulation cascades were commonly up-regulated.

To confirm further the differences in gene expression profile associated with NFT formation and neuronal cell losses, ApoD (Muffat and Walker, 2010), Npas4 (Lin et al., 2008), DCX (Moores et al., 2004), and Kcnab1 (Need et al., 2003) were selected for analysis at the protein level of up- or down-regulated genes among 24 significant genes because of the availability of antibodies. ApoD and DCX gene products had been previously suggested to be altered in AD (Thomas et al., 2003; Jin et al., 2004); however, others have not been reported.

On immunostaining, ApoD was markedly labeled in the brain of TgTauP301L with NFTs and neuronal cell losses compared with those of TgTauP301L without NFTs and neuronal cell losses. In particular, the hippocampus and white matter were markedly stained (Fig. 2b). Enhanced ApoD immunostaining was not detected in brains of TgTauP301L without NFTs and neuronal cell losses (Fig. 2a). The areas that exhibited extensive ApoD immunoreactivities were not related to those showing NFT formation and neuronal cell losses. Increased ApoD immunostaining was detected in neuronal processes, oligodendrocytes, and astrocytes (Fig. 2d) compared with that in 739 brains (Fig. 2c). Astrocytosis was also prominent in these areas. In AD and tauopathy brains, ApoD immunostaining was also detected mainly in astrocytes of the white matter and rarely in neurons in the cortex (Fig. 2f,g,i,j). ApoD was not detected in the control normal human brains (Fig. 2e,h).

Markedly decreased DCX immunoreactivities were observed in TgTauP301L showing NFTs and neuronal cell losses (Fig. 2l,n). Decrease in DCX-positive cells was observed even in areas without NFT formation. DCX-positive cells were detected in the dentate gyrus, hippocampus, and cerebral cortex of age-matched control nontransgenic mouse and TgTauP301L without NFTs and neuronal cell losses. Band-like immunoreactivities were prominent in the hippocampus of control age-matched nontransgenic mice (Fig. 2k,m). In AD and tauopathy brains, reticular immunoreactivity of DCX was markedly decreased in the dentate gyrus (Fig. 2p,q,s,t) compared with that in control human brains (Fig. 2o,r).

On Western blotting, the amount of DCX was decreased and the level of ApoD was increased in TgTauP301L mice with NFTs and neuronal cell losses compared with those in TgTauP301L without NFTs and neuronal cell losses (Fig. 3). The amounts of DCX and ApoD in sarkosyl-soluble fraction of the brain were correlated with the amount of sarkosyl-insoluble tau of the brain, suggesting that down-regulation of DCX and up-regulation of ApoD were closely associated with

TABLE I. Twenty-Four Up- and Down-Regulated Genes Shared in the Two Comparisons (517 vs. 512 and 739 vs. 736)

Description	Symbol	*P* value	Fold change (512/517)	Fold change (736/739)	Cell adhesion	Cell communication	Nervous system development	Development	Transport	Localization	DNA metabolism	Metabolism	Inflammatory response	Response to stimulus
Up-regulated														
Neuronal PAS domain protein 4	Npas4	0.03	2.33	2.77		*						*		
Thyrotropin releasing hormone	Trh	0.02	2.42	2.07		*								*
Immunoglobulin heavy chain 6 (heavy chain of IgM)	Igh-6	0.03	2.13	3.68		*			**	*		*		*
Syndecan 4	Sdc4	0.02	2.17	2.08										
Insulin receptor substrate 4	Irs4	0.02	2.11	2.10		*								
C-type lectin domain family 7, member a	Clec7a	0.04	2.21	6.62	**	*			**	*			**	*
Predicted gene 98	Gm98	0.02	3.50	2.90										
Holliday junction recognition protein	Hjurp	0.02	3.53	4.60										
Calcium/calmodulin-dependent protein kinase II inhibitor 1	Camk2n1	0.02	7.54	2.43										
Perilipin 4	Plin4	0.04	5.36	4.77										
Pyruvate dehydrogenase kinase, isoenzyme 4	Pdk4	0.03	2.80	2.28		*						*		
Proteasome (prosome, macropain) 26S subunit, ATPase 3, interacting protein	Psmc3ip	0.01	2.98	3.36							**	*		
Serine (or cysteine) peptidase inhibitor, clade A, member 3N	Serpina3n	0.02	2.65	5.47										*
Apolipoprotein D	Apod	0.03	2.05	3.55					**	*				
Periostin, osteoblast specific factor	Postn	0.02	2.01	2.23	**	*		*						
Carboxypeptidase M	Cpm	0.02	2.08	2.18								*		
Myelin-associated oligodendrocytic basic protein	Mobp	0.02	2.08	2.00										
Down-regulated														
Membrane protein, palmitoylated 4 (MAGUK p55 subfamily member 4)	Mpp4	0.01	0.40	0.29										
Pituitary tumor-transforming gene 1	Pttg1	0.00	0.09	0.11							**	*		*
Doublecortin	Dcx	0.01	0.39	0.32		*	**	*		*				
Potassium voltage-gated channel, shaker-related subfamily, beta member 1	Kcnab1	0.02	0.40	0.47					**	*				
RNA binding motif protein 45	Rbm45	0.00	0.27	0.26			**	*						
Succinate dehydrogenase complex, subunit A, flavoprotein (Fp)	Sdha	0.01	0.36	0.16					**	*		*		
RIKEN cDNA 4933400F03 gene	4933400 F03Rik	0.02	0.50	0.50										

*$P < 0.05$.

**$P < 0.01$.

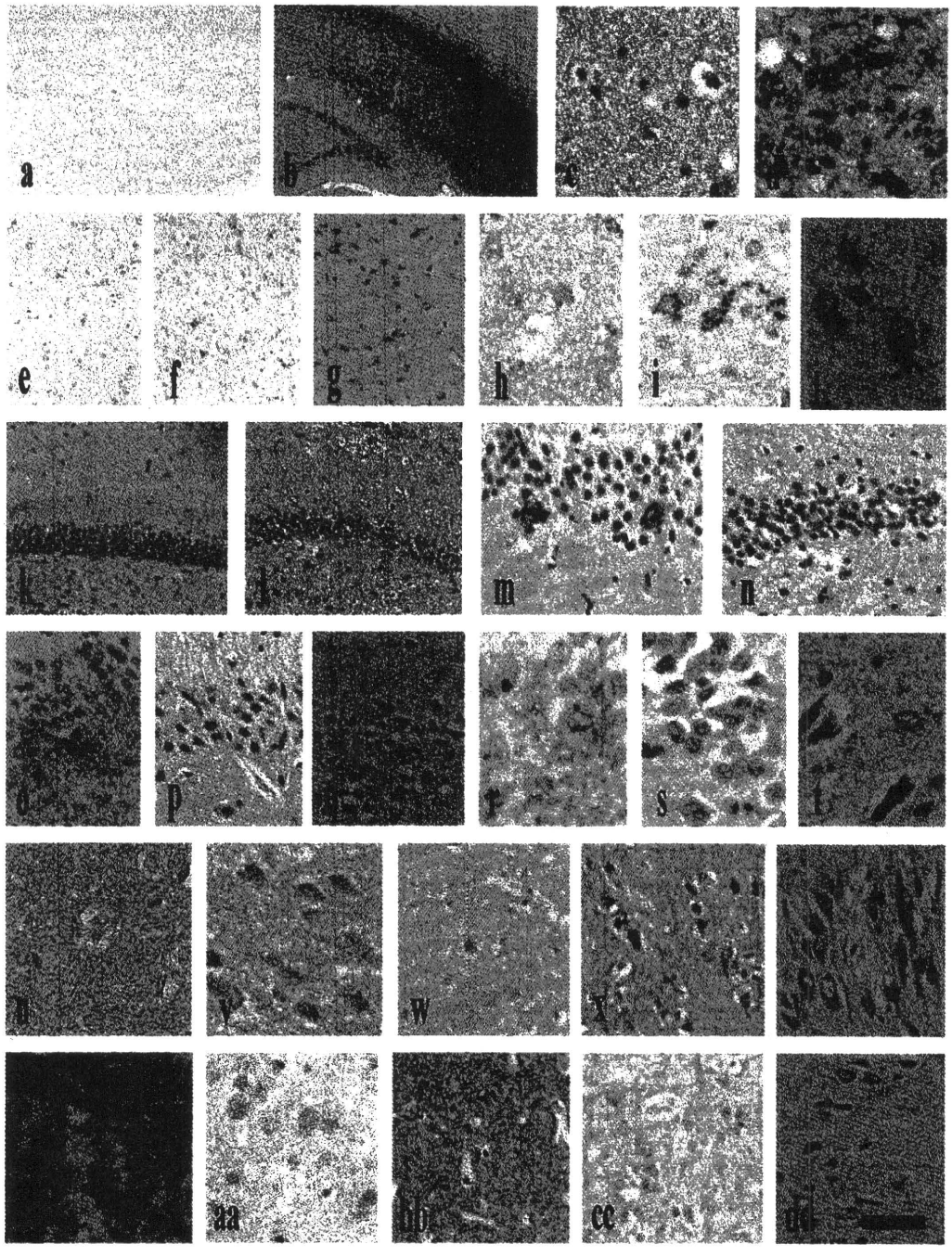

Fig. 2. Immunostaining of ApoD, DCX, Npas4, and Kcnab1. Staining of ApoD (from Patel; **a–d**), ApoD(36C6) (**e–j**), DCX (N19; **k–t**), Npas4 (polyclonal; **u–y**), and Kcnab1 (**z–dd**) in TgTauP301L without NFTs and neuronal cell losses (a,c,k,m,u,z), with NFTs and neuronal cell losses (b,d,l,n,v,aa), control human brains (e,h,o,r,w,bb), AD brains (f,i,p,s,x,cc), and FTD brains (g,j,q,t,y,dd). Staining of ApoD and Npas4 was increased in TgTauP301L brain with NFTs and neuronal cell losses, AD brains, and FTD brains compared with that in TgTauP301L brain without NFTs and neuronal cell losses and control brain. Decreased immunoreactivities of DCX and Kcnab1 were recognized in TgTauP301L brain with NFTs and neuronal cell losses, AD brain, and FTD brains. Scale bar = 50 μm in dd (applies to e–g,m–q,w–y,bb–dd); 250 μm for a,b; 100 μm for c,d,k,l; 25 μm for h–j,r–v,z,aa. [Color figure can be viewed in the online issue, which is available at wileyonlinelibrary.com.]

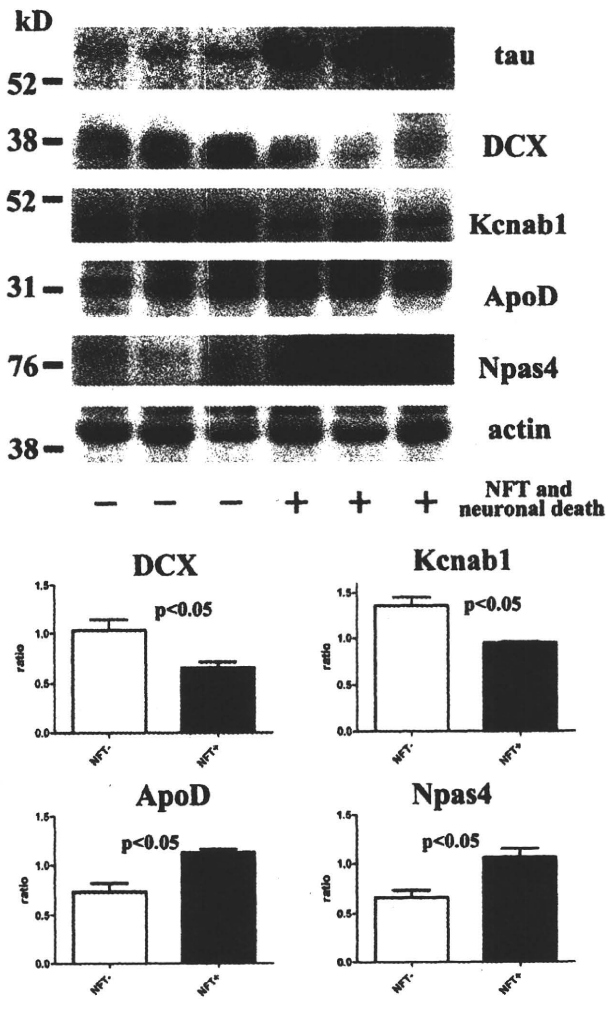

Fig. 3. Western blotting of brain extracts using tau (TAU-5), DCX (C-18), Kcnab1, ApoD, and Npas4 antibodies. Insoluble tau accumulation (TAU-5) was correlated with decreased levels of DCX (C18) and Kcnab1 and increased levels of ApoD (from Patel) and Npas4 (NBP1-06574). Plus signs indicate brain extracts of TgTauP301L with NFTs and neuronal cell losses, and minus signs indicate those of TgTauP301L without NFTs and neuronal cell losses. The signals were corrected by those of β-actin and were tested for statistical significance by using *t*-test.

NFT formation and neuronal cell losses at the gene product level (Fig. 3).

Immunostaining of Npas4 was increased in cerebral cortex and hippocampus of TgTauP301L brains with NFTs and neuronal losses (Fig. 2v) and also in AD and tauopathy brains (Fig. 2x,y). Immunoreactivity of Kcnab1 was decreased in cortex and hippocampus of TgTauP301L brains with NFTs and neuronal losses (Fig. 2aa) and also in AD and tauopathy brains (Fig. 2cc,dd). On Western blotting, the amount of Npas4 was increased and the level of Kcnab1 was decreased in TgTauP301L mice with NFTs and neuronal cell losses compared with those in TgTauP301L without NFTs and neuronal cell losses (Fig. 3). Therefore, changed expression level of Npas4 and Kcnab1 was also verified at the protein level.

DISCUSSION

Our oligonucleotide array expression study demonstrated that gene expression groups were altered in many biological pathways and that these collective alterations were closely related to the final stage of tauopathy, namely, NFT formation and neuronal cell losses. Both sets of comparisons of mice with or without NFTs and neuronal cell losses showed that five pathways including oxidative stress, apoptosis, mitochondrial fatty acid betaoxidation, inflammatory response, and complement and coagulation cascades are consistently up-regulated, suggesting that NFTs and neuronal losses occurred on the basis of at least these enhanced biological pathways with many up-regulated gene cluster expressions. Then, altered gene expression ratios demonstrated in both comparison sets consisting of 17 up-regulated genes and seven down-regulated genes and biological processes were summarized by Gene Ontology (Table I). Reported roles of up-regulated genes were classified into inhibitory synapse development (Npas4), metabolism (thyrotropin-releasing hormone, insulin receptor substrate 4, pyruvate dehydrogenase kinase, isoenzyme 4), inflammation [immunoglobulin heavy chain 6, C-type lectin domain family 7, member a, serine (or cysteine) peptidase inhibitor, clade A, member 3N, carboxypeptidase M], brain development (syndecan 4), CNS myelination (predicted gene 98, myelin-associated oligodendrocytic basic protein), cell cycle regulation (Holliday junction recognition protein), protein kinase or phosphatase activity (calcium/calmodulin-dependent protein kinase II inhibitor 1), body weight regulation (perilipin 4), proteosome system [proteasome (prosome, macropain) 26S subunit, ATPase 3, interacting protein], lipid transportation (ApoD), and tumorigenesis (periostin, osteoblast specific factor). These findings indicated that NFT formation and neuronal cell losses were associated with up-regulated conditions of CNS regeneration, metabolism, lipid transportation, proteosome function, cell cycle regulation and signaling, and inflammation. Down-regulated genes were classified into photoreceptor synaptic calcium handling (membrane protein, palmitoylated 4), neuronal protection (pituitary tumor-transforming gene 1), neurogenesis (DXC), synaptic plasticity and learning (Kcnab1), mitochondrial function (succinate dehydrogenase complex, subunit A, flavoprotein), and others (RNA binding motif protein 45, RIKEN cDNA 4933400F03 gene). These conditions can also be summarized as suppressed neuronal and synaptic function, neurogenesis, and mitochondrial dysfunction.

Among these NFTs and neuronal cell loss-related gene expressions, ApoD has been reported to be elevated in the brains and cerebrospinal fluid of AD patients

(Terrisse et al., 1998; Kalman et al., 2000). ApoD is detected in oligodendrocytes, astrocytes, neurons with NFTs, and the vicinity of senile plaques, and the level of ApoD is associated with the severity of NFTs, but not that of Aβ (Belloir et al., 2001; Glöckner and Ohm, 2003). Accumulation of ApoD has been reported in another tauopathy, Nieman Pick type C brains (Ong et al., 2002). ApoD rapidly increases with various types of brain damage and peripheral nerve regeneration (Boyles et al., 1990) and is involved in the mechanisms regulating protection from oxidative stress (Andersen, 2004; Ganfornina et al., 2008). In our study, the level of ApoD was prominently increased in the brains of mice with NFTs and neuronal cell losses as well as gene expressions. Because our mice and Nieman Pick type C patients exhibit tauopathy findings without Aβ, the increased level of ApoD appears closely related to NFT formation and neuronal cell losses. NFT-mediated neurotoxicity and increased oxidative stress may increase the level of ApoD.

We also found that the expression of DCX gene and the amount of DCX were decreased in brains with NFTs and neuronal cell losses. The level of DCX is inversely correlated with accumulation of insoluble tau aggregation. DCX is one of the microtubule-binding proteins for axonal growth and collateral branching and essential in postmitotic neurons for brain development (Moores et al., 2004; Tint et al., 2009), indicating that DCX is a marker of neurogenesis. Although a first report suggested an increased amount of DCX accompanying hippocampal neurogenesis in AD brains (Jin et al., 2004), others did not show consistent results (Boekhoorn et al., 2006a; Verwer et al., 2007). Aβ decreases the DCX-positive cells in the hippocampus in APP model mice (Zhang et al., 2007; Mirochnic et al., 2009). In tau transgenic mouse models, however, DCX-positive neurogenesis was increased in an early phase (Boekhoorn et al., 2006b; Schindowski et al., 2008). In the late stage with NFT formation, up-regulation of cell cycle events and decreased DCX levels occurred, accompanied by neuronal cell losses (Schindowski et al., 2008). These findings corresponded to our findings and suggest that suppressed neurogenesis is one of the causal factors underlying neuronal cell losses in brains with tauopathy.

Npas4 is a newly identified transcription factor that plays a role in the development of inhibitory synapses (Lin et al., 2008) and stress-induced impairment of hippocampal function (Yun et al., 2010). Kcnab1 is also associated with excitability in hippocampal neurons and impairment of learning and memory (Need et al., 2003). Altered gene expressions of both hippocampal proteins were confirmed at protein levels. Although roles of Npas4 and Kcnb1 have not been precisely clarified, our findings suggest that these novel molecules participate in cascades from tau accumulation to NFT formation and neuronal cell losses leading to memory disturbance. Thus, gene expression profile and confirmations at protein level are useful methods for clarifying the constituent molecules of tauopathy.

Recent studies in an NFT mouse model showed that NFTs are neurotoxic and cause delayed neuronal cell losses without the usual caspase-dependent apoptosis leading to acute neuronal cell losses (Spires-Jones et al., 2008; de Calignon et al., 2009). Age-dependent reinforcement of tau accumulation and mitochondrial dysfunction-related energy metabolism and oxidative stress leads to NFTs and apoptotic neuronal cell losses (Kulic et al., 2010). Given these findings, neuronal cell losses may be caused by NFT neurotoxicity, suppressed neurogenesis, and apoptosis accompanying NFT formation induced by many biological pathways. To develop therapy for neuronal cell losses as a final target of tauopathy, every step of these biological pathways and key molecules must be clarified.

ACKNOWLEDGMENTS

We thank K. Sato, M. Ono, K. Iinuma, Y. Sato, R. Tsushima, and I. Shirahama for technical assistance; Dr. Koichi Ishiguro for tau154; and Dr. Shutish C. Patel for anti-ApoD antibody.

REFERENCES

Andersen JK. 2004. Oxidative stress in neurodegeneration: cause or consequence? Nat Med 10:S18–S25.

Belloir B, Kövari E, Surini-Demiri M, Savioz A. 2001. Altered apolipoprotein D expression in the brain of patients with Alzheimer disease. J Neurosci Res 64:61–69.

Benjamini Y, Hochberg Y. 1995. Controlling the false discovery rate: a practical and powerful approach to multiple testing. J R Statist Soc B 57:289–300.

Boekhoorn K, Joels M, Lucassen PJ. 2006a. Increased proliferation reflects glial and vascular-associated changes, but not neurogenesis in the presenile Alzheimer hippocampus. Neurobiol Dis 24:1–14.

Boekhoorn K, Terwel D, Biemans B, Borghgraef P, Wiegert O, Ramakers GJ, de Vos K, Krugers H, Tomiyama T, Mori H, Joels M, van Leuven F, Lucassen PJ. 2006b. Improved long-term potentiation and memory in young tau-P301L transgenic mice before onset of hyperphosphorylation and tauopathy. J Neurosci 26:3514–3523.

Boyles JK, Notterpek LM, Anderson LJ. 1990. Accumulation of apolipoproteins in the regenerating and remyelinating mammalian peripheral nerve. Identification of apolipoprotein D, apolipoprotein A-IV, apolipoprotein E, and apolipoprotein A-I. J Biol Chem 265:17805–17815.

de Calignon A, Spires-Jones TL, Pitstick R, Carlson GA, Hyman BT. 2009. Tangle-bearing neurons survive despite disruption of membrane integrity in a mouse model of tauopathy. J Neuropathol Exp Neurol 68:757–761.

Ganfornina MD, Do Carmo S, Lora JM, Torres-Schumann S, Vogel M, Allhorn M, González C, Bastiani MJ, Rassart E, Sanchez D. 2008. Apolipoprotein D is involved in the mechanisms regulating protection from oxidative stress. Aging Cell 7:506–515.

Glöckner F, Ohm TG. 2003. Hippocampal apolipoprotein D level depends on Braak stage and APOE genotype. Neuroscience 22:103–110.

Hardy J. 2009. The amyloid hypothesis for Alzheimer's disease: a critical reappraisal. J Neurochem 110:1129–1134.

Holmes C, Boche D, Wilkinson D, Yadegarfar G, Hopkins V, Bayer A, Jones RW, Bullock R, Love S, Neal JW, Zotova E, Nicoll JA. 2008. Long-term effects of Aβ42 immunization in Alzheimer's disease: follow-up of a randomised, placebo-controlled phase I trial. Lancet 372:216–223.

Jin K, Peel AL, Mao XO, Xie L, Cottrell BA, Henshall DC, Greenberg DA. 2004. Increased hippocampal neurogenesis in Alzheimer's disease. Proc Natl Acad Sci U S A 101:343–347.

Kalman J, McConathy W, Araoz C, Kasa P, Lacko AG. 2000. Apolipoprotein D in the aging brain and in Alzheimer's dementia. Neurol Res 22:330–336.

Kim SY, Volsky DJ. 2005. PAGE: parametric analysis of gene set enrichment. BMC Bioinformatics 6:144.

Kulic L, Wollmer MA, Rhein V, Pagani L, Kuehnle K, Cattepoel S, Tracy J, Eckert A, Nitsch RM. 2010. Combined expression of tau and the Harlequin mouse mutation leads to increased mitochondrial dysfunction, tau pathology and neurodegeneration. Neurobiol Aging [E-pub ahead of print].

Lin Y, Bloodgood BL, Hauser JL, Lapan AD, Koon AC, Kim TK, Hu LS, Malik AN, Greenberg ME. 2008. Activity-dependent regulation of inhibitory synapse development by Npas4. Nature 455:1198–1204.

Mirochnic S, Wolf S, Staufenbiel M, Kempermann G. 2009. Age effects on the regulation of adult hippocampal neurogenesis by physical activity and environmental enrichment in the APP23 mouse model of Alzheimer disease. Hippocampus 19:1008–1018.

Moores CA, Perderiset M, Francis F, Chelly J, Houdusse A, Milligan RA. 2004. Mechanism of microtubule stabilization by doublecortin. Mol Cell 14:833–839.

Muffat J, Walker DW. 2010. Apolipoprotein D: an overview of its role in aging and age-related diseases. Cell Cycle 9:269–273.

Murakami T, Paitel E, Kawarabayashi T, Ikeda M, Chishti MA, Janus C, Matsubara E, Sasaki A, Kawarai T, Phinney AL, Harigaya Y, Horne P, Egashira N, Mishima K, Hanna A, Yang J, Iwasaki K, Takahashi M, Fujiwara M, Ishiguro K, Bergeron C, Carlson GA, Abe K, Westaway D, St. George-Hyslop P, Shoji M. 2006. Cortical neuronal and glial pathology in TgTauP301L transgenic mice: neuronal degeneration, memory disturbance, and phenotypic variation. Am J Pathol 169:1365–1375.

Need AC, Irvine EE, Giese KP. 2003. Learning and memory impairments in $K_v\beta1.1$-null mutants are rescued by environmental enrichment or ageing. Eur J Neurosci 18:1640–1644.

Ong WY, Hu CY, Patel SC. 2002. Apolipoprotein D in the Niemann-Pick type C disease mouse brain: an ultrastructural immunocytochemical analysis. J Neurocytol 31:121–129.

Paquet D, Bhat R, Sydow A, Mandelkow EM, Berg S, Hellberg S, Fälting J, Distel M, Köster RW, Schmid B, Haass C. 2009. A zebrafish model of tauopathy allows in vivo imaging of neuronal cell death and drug evaluation. J Clin Invest 119:1382–1395.

Patel SC, Asotra K, Patel YC, McConathy WJ, Patel RC, Suresh S. 1995. Astrocytes synthesize and secrete the lipophilic ligand carrier apolipoprotein D. Neuroreport 6:653–657.

Santacruz K, Lewis J, Spires T, Paulson J, Kotilinek L, Ingelsson M, Guimaraes A, DeTure M, Ramsden M, McGowan E, Forster C, Yue M, Orne J, Janus C, Mariash A, Kuskowski M, Hyman B, Hutton M, Ashe KH. 2005. Tau suppression in a neurodegenerative mouse model improves memory function. Science 309:476–481.

Schindowski K, Belarbi K, Bretteville A, Ando K, Buée L. 2008. Neurogenesis and cell cycle-reactivated neuronal death during pathogenic tau aggregation. Genes Brain Behav 7:92–100.

Smyth GK. 2004. Linear models and empirical bayes methods for assessing differential expression in microarray experiments. Stat Appl Genet Mol Biol 3:Article 3.

Spires-Jones TL, de Calignon A, Matsui T, Zehr C, Pitstick R, Wu HY, Osetek JD, Jones PB, Bacskai BJ, Feany MB, Carlson GA, Ashe KH, Lewis J, Hyman BT. 2008. In vivo imaging reveals dissociation between caspase activation and acute neuronal death in tangle-bearing neurons. J Neurosci 28:862–867.

Spires-Jones TL, Stoothoff WH, de Calignon A, Jones PB, Hyman BT. 2009. Tau pathophysiology in neurodegeneration: a tangled issue. Trends Neurosci 32:150–159.

Stokin GB, Lillo C, Falzone TL, Brusch RG, Rockenstein E, Mount SL, Raman R, Davies P, Masliah E, Williams DS, Goldstein LS. 2005. Axonopathy and transport deficits early in the pathogenesis of Alzheimer's disease. Science 307:1282–1288.

Terrisse L, Poirier J, Bertrand P, Merched A, Visvikis S, Siest G, Milne R, Rassart E. 1998. Increased levels of apolipoprotein D in cerebrospinal fluid and hippocampus of Alzheimer's patients. J Neurochem 71:1643–1650.

Thomas EA, Laws SM, Sutcliffe JG, Harper C, Dean B, McClean C, Masters C, Lautenschlager N, Gandy SE, Martins RN. 2003. Apolipoprotein D levels are elevated in prefrontal cortex of subjects with Alzheimer's disease: no relation to apolipoprotein E expression or genotype. Biol Psychiatry 54:136–141.

Tint I, Jean D, Baas PW, Black MM. 2009. Doublecortin associates with microtubules preferentially in regions of the axon displaying actin-rich protrusive structures. J Neurosci 29:10995–11010.

Verwer RW, Sluiter AA, Balesar RA, Baayen JC, Noske DP, Dirven CM, Wouda J, van Dam AM, Lucassen PJ, Swaab DF. 2007. Mature astrocytes in the adult human neocortex express the early neuronal marker doublecortin. Brain 130:3321–3335.

Yun J, Koike H, Ibi D, Toth E, Mizoguchi H, Nitta A, Yoneyama M, Ogita K, Yoneda Y, Nabeshima T, Nagai T, Yamada K. 2010. Chronic restraint stress impairs neurogenesis and hippocampus-dependent fear memory in mice: possible involvement of a brain-specific transcription factor Npas4. J Neurochem 114:1840–1851.

Zhang C, McNeil E, Dressler L, Siman R. 2007. Long-lasting impairment in hippocampal neurogenesis associated with amyloid deposition in a knock-in mouse model of familial Alzheimer's disease. Exp Neurol 204:77–87.

EXPERT REVIEWS

Secretase inhibitors and modulators for Alzheimer's disease treatment

Expert Rev. Neurother. 9(5), 661–679 (2009)

Taisuke Tomita
Department of Neuropathology and Neuroscience, Graduate School of Pharmaceutical Sciences, The University of Tokyo, Bunkyo, Tokyo 113-0033, Japan
Tel.: +81 358 414 868
Fax: +81 358 414 708
taisuke@mol.f.u-tokyo.ac.jp

Genetic and biological studies provide strong evidence that the deposition of amyloid-β peptide (Aβ) contributes to the etiology of Alzheimer's disease (AD). Aβ is generated from amyloid-β precursor protein by β- and γ-secretases, which are plausible molecular targets for AD treatment. Thus, drugs that regulate the production of Aβ by inhibiting or modulating secretase activity could provide effective therapeutics for AD. Both secretases are transmembrane proteases: β-site amyloid-β precursor protein cleaving enzyme 1, the main neuronal β-secretase, is a single span transmembrane aspartyl protease; γ-secretase is a multiprotein complex comprising four core subunits that are all transmembrane proteins: presenilin, nicastrin, anterior pharynx-defective 1 and presenilin enhancer 2. Molecular biochemical, enzymological and genetic analyses reveal the molecular mechanisms of these secretases in the generation of Aβ. Moreover, extensive drug screening and development have enabled some secretase inhibitors and modulators to advance into late-Phase clinical trials. This review focuses on recent progresses in β- and γ-secretase biology, including the proteolytic mechanism, regulation and composition of these enzymes. Moreover, this review discusses the recent development of inhibitors, and provides a direction for the effective treatment of AD through inhibition/modulation of β- and γ-secretase activities.

Keywords: Alzheimer's disease • amyloid-β protein • amyloid precursor protein • Notch • secretase • lipid raft • inhibitor • modulator • vesicle trafficking

Alzheimer's disease (AD) is a progressive, dementing neurodegenerative disorder affecting over 27 million people worldwide in 2006 [1,2]. As the average age of the population increases, the number of AD patients is expected to quadruple by 2050. This fatal brain disease was first described by German psychiatrist Alois Alzheimer in 1906. He reported the deposition of two abnormal structures, termed senile plaques and neurofibrillary tangles, in the brain of Auguste D, who suffered from dementia. Now these abnormalities are thought to be prime suspects in damaging and killing neurons in affected patients. Senile plaques, which are deposited in the extracellular space of brain parenchyma, primarily contain amyloid-β peptides (Aβ) that are proteolytically produced from amyloid-β precursor protein (APP) (Figure 1) [2]. Neurofibrillary tangles are formed within the neuronal cytoplasm and are composed of filaments of hyperphosphorylated forms of the microtubule-associated protein tau [3]. Immunohistochemical studies suggest that the primary pathological event in AD brains is the deposition of Aβ as senile plaques [2]. By contrast, the appearance of neurofibrillary tangles correlates with the neuronal loss [2,3]. Moreover, the deposition of the patients with aggregated tau is observed in brains of other types of dementia (e.g., frontotemporal dementia [FTD]). Thus, both Aβ and tau are thought to be crucial to the etiology of AD and neuronal death, respectively.

Pathomechanisms of AD

Identification and analyses of the genes causative to familial AD (FAD) accelerated the understanding of the molecular pathology of AD [4]. The majority of newly synthesized APP is proteolytically processed by α-secretase to release a soluble large extracellular domain (soluble APPα) and small C-terminal stub (C83). To date, several A disintegrin and metalloprotease domain protein (ADAM) proteases have been found as α-secretase: as TNF-α converting enzyme (TACE or ADAM17), ADAM9 and ADAM10 [5]. However, some fraction of APP is cleaved

 10.1586/ERN.09.24 ISSN 1473-7175

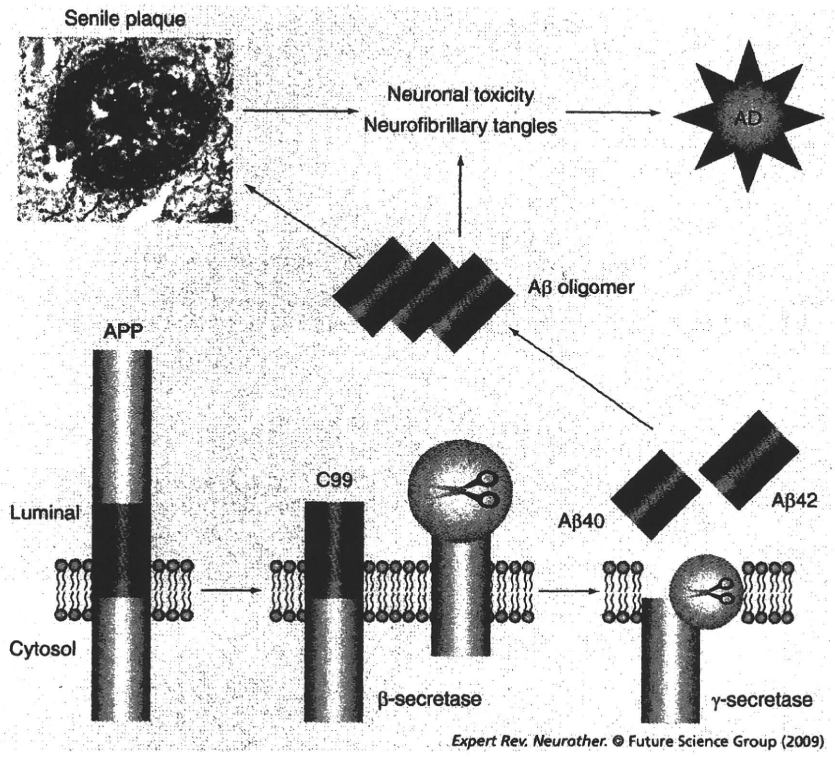

Figure 1. Amyloidogenic processing of APP and the amyloid hypothesis. The ectodomain of APP is first shed by β-secretase. Alternatively, APP can be cut within the Aβ sequence by α-secretase (not shown). The C-terminal stub (C99) is then cleaved by γ-secretase to release Aβ. Aggregated Aβ oligomers form senile plaques and/or mediate neuronal toxicity to cause AD.
Aβ: Amyloid-β peptide; AD: Alzheimer's disease; APP: Amyloid-β precursor protein.

by β-secretase at more distal sites to the membrane to generate soluble APPβ and a longer C-terminal stub, C99. The remaining C-terminal stubs are subsequently cleaved by γ-secretase within the transmembrane domain (TMD). γ-secretase-mediated cleavage of C99 resulted in the generation of Aβ, while C83 is processed to release the shorter nontoxic peptide, p3. The C-terminal length of Aβ generated by γ-secretase is heterogeneous: Aβ40, composed of a 40-amino acid peptide is the major species of the Aβ secreted from cells; while Aβ42 with two more amino acids is a relatively minor molecular species [6,7]. However, Aβ42 is the initially and predominantly deposited Aβ species in AD brains [8], and aggregates much faster than the more common Aβ40 species [9]. Importantly, all genetic mutations in the *APP* gene that cosegregate with affected members in FAD pedigrees increase production of the amyloidogenic Aβ42 species or aggregability of Aβ peptides [2,4]. The Swedish mutation located at most N-terminal sides of Aβ caused a drastic overproduction in Aβ generation by the increase in the β-secretase-mediated cleavage [10,11]. Furthermore, several mutations located near the C-terminus of Aβ caused a selective increase in the generation of Aβ42 by affecting γ-secretase activity [6]. By contrast, point mutations located within the Aβ sequence showed no effect on the production, but increased the aggregability of this amyloidogenic peptide [12]. Finally, genetic studies of gene copy number variation revealed that the duplication of *APP* gene is linked to FAD, suggesting that the levels of aggregated Aβ in the brain is the rate-limiting factor for the onset of AD [13]. By contrast, mutations in the *tau* gene are linked to familial FTD without the deposition of senile plaques [3], supporting the notion, based on pathology, that tau is directly involved in neurodegeneration. These genetic and biochemical data indicate that Aβ is the real molecular culprit that underlies the pathogenesis of AD (the 'amyloid hypothesis') [14].

Molecular identity of the secretases for amyloidogenic processing

Based on the amyloid hypothesis, drugs that can prevent production, aggregation and deposition of Aβ are thought to be promising therapeutics for AD [2,15]. Much attention has been focused on the inhibition or modulation of activities of β- and γ-secretases as disease-modifying therapies based on pathological mechanisms [16–21]. In particular, the amyloidogenic pathway in neurons is initiated by β-secretase cleavage. Thus, the elucidation of the molecular identity of β-secretase had been one of the key issues for the development of AD therapeutics [22,23]. In fact, identification of β-site APP cleaving enzyme (BACE)1 was reported mainly by pharmaceutical companies with different strategies [24–28]. All results led to the same conclusion: a single span transmembrane glycolprotein, BACE1, that harbors an aspartic protease domain at the extracellular side, is responsible for β-secretase activity. Genetic ablation of *BACE1* caused complete loss of Aβ and C99, as well as sAPPβ generation in mouse brains, supporting the notion that BACE1 itself is β-secretase [29–31]. To date, several proteins have been implicated as BACE1-binding partners. However, the recombinant extracellular domain of BACE1 harbors β-secretase activity in *in vitro* assays, implicating that BACE1 functions as a protease by itself. Growing evidence suggests that the levels and/or activity of BACE1 are increased in AD patients, yet no FAD-linked mutation in the *BACE1* gene has been reported [32–35]. A link between BACE1 levels, Aβ load and AD pathology has been reported [36], suggesting that increased BACE1 expression is indeed an important risk factor for sporadic AD. Intriguingly, recent analyses revealed that the levels of BACE1 protein are regulated at multiple levels in the biosynthetic pathway (see later).

Compared with β-secretase, γ-secretase has remained a mystery for a long time, as γ-secretase endoproteolyzes a scissile bond within the hydrophobic membrane-embedded TMD of APP [37]. Historically, clues regarding the molecular identity of γ-secretase were first obtained from genetic studies of FAD patients. After